

Grassmannian Learning: Embedding Geometry Awareness in Shallow and Deep Learning

Jiayao Zhang, Guangxu Zhu, Robert W. Heath Jr., and Kaibin Huang

Modern machine learning algorithms have been adopted in a range of signal-processing applications spanning computer vision, natural language processing, and artificial intelligence. Many relevant problems involve subspace-structured features, orthogonality constrained or low-rank constrained objective functions, or subspace distances. These mathematical characteristics are expressed naturally using the Grassmann manifold. Unfortunately, this fact is not yet explored in many traditional learning algorithms. In the last few years, there have been growing interests in studying Grassmann manifold to tackle new learning problems. Such attempts have been reassured by substantial performance improvements in both classic learning and learning using deep neural networks. We term the former as *shallow* and the latter *deep* Grassmannian learning. The aim of this paper is to introduce the emerging area of Grassmannian learning by surveying common mathematical problems and primary solution approaches, and overviewing various applications. We hope to inspire practitioners in different fields to adopt the powerful tool of Grassmannian learning in their research.

I. OVERVIEW OF GRASSMANN LEARNING

A Grassmann manifold refers to a space of subspaces embedded in a higher-dimensional vector space (e.g., the surface of a sphere in a 3D space). The mathematical notation arises in a variety of science and engineering applications in the areas of computer vision, statistical learning, wireless communications, and natural language processing. In visual recognition and classification tasks, the Grassmann manifold is used to model the invariant illumination or pose space [1, 2]. In statistical learning, novel methods such as Grassmannian discriminant analysis [3, 4, 5] and clustering [6, 7] are developed for processing data on the Grassmann manifold or exploiting tools from Grassmannian optimization to enhance learning performance. In recommender systems, under low-rank or sparsity constraints, the problem of matrix completion can be solved using Grassmannian learning methods [8, 9]. In wireless communications, Grassmannian packing can be applied to the design of space-time constellations [10, 11, 12] and that of limited feedback beamforming codebook [13, 14]. In natural language processing, the Grassmann manifold can be used to model affine subspaces in document-specific language models

[15]. These problems generally utilize the Grassmann manifold as a tool for nonlinear dimensionality reduction or to tackle optimization objectives that are *invariant to the basis of domain*. This approach is not yet explored in other learning algorithms. The set of mentioned problems belong to *shallow learning* and will be surveyed in the first half of this paper. In the second half of the paper, we will discuss the latest trends in utilizing Grassmann manifolds to exploit the geometry of problems for deep learning [16, 17]. Relevant applications include shape alignment and retrieval [18], geodesic convolutional neural nets [19], and Riemannian curvature in neural networks [20]. Researchers have also proposed new deep neural network architectures for coping with data on the Grassmann manifold [21, 22].

The strength of Grassmannian learning lies in its capability to harness the structural information embedded in the problem, leading to lower complexity and improved performance. For example, the *Grassmannian discriminant analysis* (GDA) applied to image-set classification can better capture the subspace invariance of facial expressions than traditional methods do. As another example, in visual domain adaptation, *Grassmannian geodesic flow kernel* (GFK) can exploit the domain-invariant features hidden in the geodesic (defined in Section IV-A) connecting the source and target domains, both being Grassmann manifolds, to enable effective knowledge transfer between them. More evident examples are provided in the sequel. As we observe, the relevant techniques are scattered in diverse fields, and there lacks a systematic and accessible introduction to the Grassmann learning. The existing introductory work is either mathematically involved [26, 27, 28] or is documentation for software packages [29, 30]. For these reasons, we aim to provide an introduction to the Grassmannian manifold and its applications to both shallow and deep learning. To this end, two common paradigms in Grassmannian learning, namely, the *Grassmannian kernel methods* and the *Grassmannian optimization*, are introduced. Representative applications in these two paradigms are surveyed and summarized in Table I. We hope the discussion will facilitate readers in the signal processing community to tackle problems similar in nature.

II. A CRASH COURSE ON GRASSMANN MANIFOLDS

This section introduces notions from differential geometry, and then correlates them to the main theory. A more comprehensive and rigorous treatment can be found in [31, 32]. The notation used in this paper is summarized in Table II for ease of exposition.

J. Zhang is with the Dept. of Computer Science, and G. Zhu and K. Huang with the Dept. of Electrical & Electronic Engr., all at The University of Hong Kong, Hong Kong. R. W. Heath Jr. is with the Dept. of Electrical & Computer Engr. at The University of Texas at Austin, TX, USA. Corresponding author: J. Zhang <jiaoyaozhang@acm.org>.

Model	Learning Methods	Paradigm
Shallow	Grassmannian Discriminant Analysis (GDA) [3] (Section III-A)	Kernel Method
	Sparse Spectral Clustering (SSC) [7] (Section III-B)	Grassmannian Optimization
	Low-rank Matrix Completion [8] (Section III-C)	Grassmannian Optimization
Deep	Sample Geodesic Flow (SGF) [23] with Deep Features (Section IV-A)	Grassmannian Optimization
	Geodesic Flow Kernel (GFK) [24] with Deep Features (Section IV-A)	Kernel Method
	Building deep neural nets on the Grassmann manifold [21, 25] (Section IV-B)	Grassmannian Optimization

TABLE I: Summary of representative Grassmannian learning methods.

Notation	Remark
$\mathbb{R}^n, \mathbb{C}^n$	n -dimensional real and complex space
\mathcal{M}, \mathcal{H}	Arbitrary manifolds
$\mathcal{G}(n, k)$	(n, k) -Grassmann manifold
$\mathbf{O}(k)$	Collection of $k \times k$ orthonormal (or unitary in the complex case) matrix
$x, \mathbf{x}, \mathbf{X}$	Scalar, vector, matrix or matrix representation of points on the Grassmann manifold
$\mathcal{T}_{\mathbf{X}}, \Delta$	Tangent space and tangent vector of \mathcal{M} at \mathbf{X}
$\Phi(\cdot)$	Geodesic on the manifold
\exp, \log	Exponential and logarithm maps
θ_i	Principal angle
$F_{\mathbf{X}}$	Matrix derivative of some function F with respect to \mathbf{X}
$\nabla_{\mathbf{X}} F$	Gradient of F at point \mathbf{X}
$d(\cdot, \cdot)$	A distance measure
$k(\cdot, \cdot)$	A kernel function
CS Decomposition	Cosine-Sine Decomposition (Section II-D)
SPD	Symmetric Positive Definite (Section II-E)
RKHS	Reproducing Kernel Hilbert Space (Section II-F)

TABLE II: List of notations used in this paper.

A. Definition of Grassmann Manifold

The Grassmann manifold $\mathcal{G}(n, k)$ with the integers $n \geq k > 0$ is the space formed by all k -dimensional linear subspaces embedded in an n -dimensional real or complex Euclidean space. As illustrated in Fig. 1, the space of all lines passing through the origin in \mathbb{R}^2 plane forms the real $\mathcal{G}(3, 1)$. Representation of elements on the Grassmann manifold is important for developing learning algorithms. An element on a Grassmann manifold is typically represented an arbitrarily chosen $n \times k$ orthonormal matrix \mathbf{X} whose column spans the corresponding subspace, called a *generator* of the element. The Grassmann manifold can be represented by a collection of such generator matrices. Mathematically, this may be written as

$$\mathcal{G}(n, k) = \left\{ \text{span}(\mathbf{X}) : \mathbf{X} \in \mathbb{R}^{n \times k}, \mathbf{X}^\top \mathbf{X} = \mathbf{I}_k \right\}. \quad (1)$$

In our discussion, we will use \mathbf{X} to represent a point on the Grassmann manifold [$\mathbf{X} \in \mathcal{G}(n, k)$], a subspace, or a orthonormal matrix ($\mathbf{X}^\top \mathbf{X} = \mathbf{I}$). The specific meaning will be clear in the context. Let $\mathbf{O}(k)$ denote the collections of all $k \times k$ orthonormal matrices. Since a subspace is represented by the span of the columns of \mathbf{X} , an element on the Grassmann manifold is invariant to rotations. Specifically, \mathbf{X} and $\mathbf{X}\mathbf{R}$ correspond to the same point on $\mathcal{G}(n, k)$ for any $\mathbf{R} \in \mathbf{O}(k)$.

B. Principal Angle

The distance between two elements $\mathbf{X}, \mathbf{Y} \in \mathcal{G}(n, k)$ on the Grassmann manifold is a function of the *principal angles*

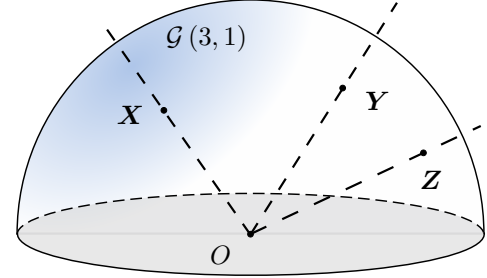


Fig. 1: Example of a Grassmann manifold. The Grassmann manifold $\mathcal{G}(3, 1)$ is the collection of lines in the Euclidean space \mathbb{R}^3 . The elements on $\mathcal{G}(3, 1)$ are represented by points such as \mathbf{X}, \mathbf{Y} and \mathbf{Z} , at the interceptions of the corresponding lines and the surface of the unit sphere in \mathbb{R}^3 .

$\{\theta_i\}_{i=1}^k$. The principal angles can be defined recursively by

$$\begin{cases} \cos \theta_i = \max_{\substack{\mathbf{x}_i \in \mathbf{X} \\ \mathbf{y}_i \in \mathbf{Y}}} \mathbf{x}_i^\top \mathbf{y}_i \\ \mathbf{x}_i^\top \mathbf{x}_i = 1, \quad \mathbf{y}_i^\top \mathbf{y}_i = 1, \\ \mathbf{x}_i^\top \mathbf{x}_j = 0, \quad \mathbf{y}_i^\top \mathbf{y}_j = 0, \quad \forall j < i, \end{cases} \quad (2)$$

for all $i = 1, 2, \dots, k$. Intuitively, principal angles are the “minimal” angles between all possible bases of two subspaces. In practice, the principal angles between $\mathbf{X}, \mathbf{Y} \in \mathcal{G}(n, k)$ can be computed from singular value decomposition (SVD), where the singular values of $\mathbf{X}^\top \mathbf{Y}$ are the cosines of the principal angles. We will show how different distance measures can be defined using the principal angles shortly in Section II-E.

C. Tangent Space, Gradient and Retraction

Gradient-based learning algorithms on the Grassmann manifold require the notion of tangency. For a point $\mathbf{X} \in \mathcal{G}(n, k)$, the space of tangent vectors $\mathcal{T}_{\mathbf{X}}$ at \mathbf{X} is defined as the set of all “vectors” (matrices with a sense of direction to be precise) $\{\Delta\}$ such that $\mathbf{X}^\top \Delta = \mathbf{0}$. The gradient of some function $F : \mathcal{G}(n, k) \rightarrow \mathbb{R}$ defined on a Grassmann manifold can be computed by projecting the “Euclidean gradient” $\mathbf{F}_{\mathbf{X}} = \left[\frac{\partial F}{\partial \mathbf{X}_{ij}} \right]$ onto the tangent space of the Grassmann manifold via the orthogonal projection $\mathbf{F}_{\mathbf{X}} \rightarrow \nabla_{\mathbf{X}} F$:

$$\nabla_{\mathbf{X}} F = (\mathbf{I}_k - \mathbf{X} \mathbf{X}^\top) \mathbf{F}_{\mathbf{X}}. \quad (3)$$

Since $(\mathbf{I} - \mathbf{X} \mathbf{X}^\top)$ is an orthogonal projection onto the orthogonal complement of \mathbf{X} , $\nabla F_{\mathbf{X}}^\top \mathbf{X} = \mathbf{0}$ and hence $\nabla F_{\mathbf{X}}$ is a tangent vector. The gradient computation in (3) plays an important role in Grassmannian optimization algorithms such as conjugate gradient descent. Such algorithms aim at finding the tangent matrix corresponding to the descent direction and computing a step forward on the manifold aligned in this direction. This requires an “retraction” operation mapping a tangent matrix back onto the manifold through the exponential map, which will be defined explicitly after introducing the concept of geodesic.

D. Grassmann Geodesic

Given two points on a manifold, a geodesic refers to the shortest curve on the manifold connecting the points. Consider the earth as an example. Mathematically, the earth surface is a manifold, namely a two dimensional sphere embedded in the three dimensional Euclidean space, and geodesics are arcs on the great circles of the earth. The trajectories of airliners or sea carriers are conveniently represented as “straight lines” on a global map, but they in fact travel on on great circles of the earth when viewed from the outer space. Then the geodesic between a origin and a destination is the connecting arc on a great circle passing the two points. Solving for geodesic is a classical problem in the calculus of variation. In the case of the Grassmann manifold, there exists relatively simple method of computing geodesics using the relatively simple method based on the SVD [26, 27, 28].

Computing Grassmannian Geodesic: The geodesic between two points $\mathbf{X}, \mathbf{Y} \in \mathcal{G}(n, k)$ may be parametrized by a function $\Phi(t) : [0, 1] \rightarrow \mathcal{G}(n, k)$, where $\Phi(0) = \mathbf{X}$ and $\Phi(1) = \mathbf{Y}$. The parameter $t \in [0, 1]$ controls the location on the geodesic and $t = \{0, 1\}$ corresponds to the two end points. To compute the geodesic on the Grassmannian, consider the following operations. First, transport the point \mathbf{X} (a subspace) in the Euclidean space with the direction and distance as specified by the tangent vector $\Delta \in \mathcal{T}_{\mathbf{X}}$. Second, project the displaced point onto the manifold $\mathcal{G}(n, k)$, giving the destination \mathbf{Y} . This particular “projection” operation is the exponential mapping mentioned in Section II-C and to be defined in the sequel. Note that \mathbf{Y} thus obtained is a subspace resulting from rotating \mathbf{X} in the direction Δ . Given the above

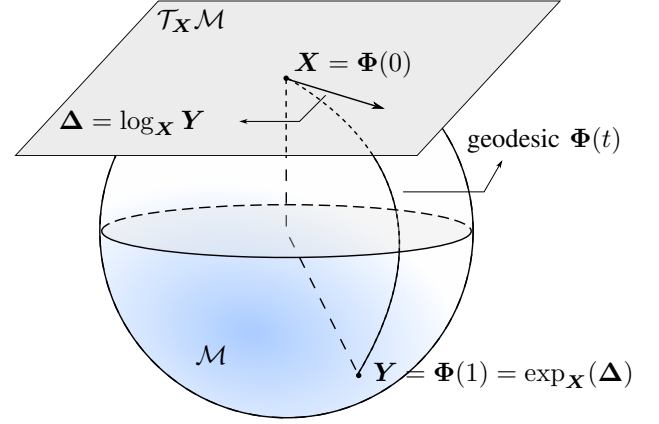


Fig. 2: Consider two points \mathbf{X} and \mathbf{Y} on the Grassmann manifold represented by the sphere. The figure illustrates the tangent space at \mathbf{X} denoted as $\mathcal{T}_{\mathbf{X}} \mathcal{M}$, the geodesic $\Phi(t)$ connecting \mathbf{X} and \mathbf{Y} , the logarithm map maps the tangent vector Δ to the point on the manifold whereas the exponential map does the reverse.

operation and $\mathbf{U} \Sigma \mathbf{V}^\top$ being the compact SVD of Δ , the Grassmann geodesic between \mathbf{X} and \mathbf{Y} can be written as

$$\Phi(t) = [\mathbf{X} \mathbf{V} \quad \mathbf{U}] \begin{bmatrix} \text{diag}(\cos \Sigma t) \\ \text{diag}(\sin \Sigma t) \end{bmatrix} \mathbf{V}^\top. \quad (4)$$

where the sine and cosine act elementwisely on the diagonal of Σ (i.e., the singular values of Δ). One can verify that \mathbf{X} and \mathbf{Y} are two end points of the geodesic: $\mathbf{X} = \Phi(0)$ and $\mathbf{Y} = \Phi(1)$. Then the exponential map, denoted as $\exp : \mathcal{T}_{\mathbf{X}} \rightarrow \mathcal{G}(n, k)$, can be defined as the computation of $\mathbf{Y} = \Phi(1)$ using the origin \mathbf{X} and the tangent Δ .

How can we compute the Grassmann geodesic without the knowledge of the tangent vector? In this case, the *Cosine-Sine* (CS) decomposition is a tool that can compute the vector Δ pointing in the direction from \mathbf{X} , a point on the Grassmannian $\mathcal{G}(n, k)$, to another \mathbf{Y} . For the two points \mathbf{X} and \mathbf{Y} , the CS decomposition can be viewed as the inverse mapping of the exponential map from Δ to \mathbf{Y} , which is thus referred in the literature as the *logarithm map* $\log_{\mathbf{X}} \mathbf{Y} : \mathcal{G}(n, k) \rightarrow \mathcal{T}_{\mathbf{X}}$. Mathematically, the decomposition can be defined using the following equation:

$$\begin{bmatrix} \mathbf{X}^\top \mathbf{Y} \\ (\mathbf{I}_n - \mathbf{X} \mathbf{X}^\top) \mathbf{Y} \end{bmatrix} = \begin{bmatrix} \mathbf{V} \cos(\Sigma) \mathbf{V}^\top \\ \mathbf{U} \sin(\Sigma) \mathbf{V}^\top \end{bmatrix}, \quad (5)$$

for some orthonormal matrices $\mathbf{U} \in \mathbf{O}(n)$ and $\mathbf{V} \in \mathbf{O}(k)$. Then the logarithm map can be defined as $\log_{\mathbf{X}} : \mathbf{Y} \mapsto \Delta$ with $\Delta = \mathbf{U} \Sigma \mathbf{V}^\top$. In practice, the CS decomposition can be implemented based on the generalized SVD [26] which computes the pair of SVD in (5). To summarize, we illustrate the quantities discussed above in Fig. 2. We will consider an example later in Section IV in the context of transfer learning.

E. Subspace Distance Measures

Many machine learning algorithms require measuring the similarity between data samples. For example, in computer vision, the similarity between two images may be measured

by the sum of squared differences of each pixel, the variation in the histogram of feature descriptors, the difference in the latent representation, and many more. Similarly, in the applications involving Grassmannian data, characterization of the discrepancy between subspaces are usually needed. In the literature, many subspace-distance measures have been defined and used, including the arc length (corresponding to the geodesic distance) d , Fubini-Study distance d_{FS} , chordal distance d_{C} , projection distance d_{P} , and Binet-Cauchy distance d_{BD} . In algorithmic design and analysis, a specific subspace distance measure is chosen either for tractability or performance optimization. The mathematical definitions of some commonly used measures are summarized in Table III. The definitions reveal two ways of computing the subspace distances between two points \mathbf{X} and \mathbf{Y} on the Grassmannian: one is in terms of their principal angles $\{\theta_i\}_{i=1}^k$ and the other based on the orthonormal matrices \mathbf{X} and \mathbf{Y} . Furthermore, as shown in the table, the projection and Binet-Cauchy distances also have their kernel-based definitions. More relevant details are given in the subsequent discussion on kernel methods.

The subtle differences between various measures can be explained intuitively as follows. The arc length is the length of the Grassmann geodesic and the longest among all distances. The chordal and projection distances both involve embedding the Grassmann manifold in higher dimensional Euclidean spaces and consider the familiar F-norm therein (other norms such as 2-norms may also be used, which leads to e.g., projection 2-norm). For example, the chordal distance embeds the Grassmann manifold $\mathcal{G}(n, k)$ in the $(n \times k)$ -dimensional Euclidean space while the projection distance embeds $\mathcal{G}(n, k)$ in the $n \times n$ Symmetric Positive-Definite (SPD) manifold, formed by real $n \times n$ SPD matrices. A distance defined in a higher dimensional ambient space tends to be *shorter* since “cutting a shorter path” is possible. For example, a chord is short than an arc between the same two points. Mathematically, we have the following inequalities among several distance measures [26]: for any $\mathbf{X}, \mathbf{Y} \in \mathcal{G}(n, k)$,

$$d(\mathbf{X}, \mathbf{Y}) > d_{\text{C}}(\mathbf{X}, \mathbf{Y}) > d_{\text{P}}(\mathbf{X}, \mathbf{Y}), d(\mathbf{X}, \mathbf{Y}) > d_{\text{FS}}(\mathbf{X}, \mathbf{Y}). \quad (6)$$

Note the chordal distance can be rewritten as $d_{\text{C}} = \sqrt{2} \left(\sum_{i=1}^k \sin^2 \frac{\theta_i}{2} \right)^{1/2}$. It is worth mentioning that removing $\sqrt{2}$ in the above expression gives another distance measure, the *Procrustes distance*, frequently used in shape analysis [33]. For illustration, we provide two examples in Example 1.

F. Grassmann Kernel Methods

1) *Background on Kernel Methods*: In many machine learning applications, to better explore the latent data structure, a common practice is to project data into some high-dimensional feature space through a specific mapping and train the model there. It is expected that the low-dimensional data can be better disentangled in the higher dimension where the data structure is more clear. However, such training involves the computation of the coordinates of the projected data samples and their pairwise distances all in the high-dimensional feature space, resulting in high computation complexity.

The kernel method overcomes the difficulties by introducing a kernel function $k(\cdot, \cdot)$ associated with a corresponding mapping $\phi(\cdot)$. This pair of functions induces a specific high-dimensional feature space. A Kernel method allows us to efficiently compute the similarity between two data samples in the feature space without the need to compute $\phi(\cdot)$ explicitly, which is in general difficult and in some cases intractable. The mathematical principle of kernel methods are as follows. The kernel function $k(\cdot, \cdot)$ and the mapping $\phi(\cdot)$ uniquely determine a *reproducing kernel Hilbert space* (RKHS), which is a vector space endowed with a proper inner product, denoted as $\langle \cdot, \cdot \rangle_{\mathcal{H}}$, and satisfying a reproducing property. Mathematically, $k(\mathbf{x}, \mathbf{y}) = \langle \mathbf{x}, \mathbf{y} \rangle_{\mathcal{H}} = \phi(\mathbf{x})^\top \phi(\mathbf{y})$. Exploiting the property, the dimensionality-sensitive operation of inner-product involved in the distance evaluation in the high-dimension feature space, denoted as $d_{\mathcal{H}}^2(\cdot, \cdot)$, can be replaced by the evaluation of the computationally-friendly kernel function. This exploits the following mathematical relation:

$$\begin{aligned} d_{\mathcal{H}}^2(\mathbf{x}, \mathbf{y}) &= \phi(\mathbf{x})^\top \phi(\mathbf{x}) + \phi(\mathbf{y})^\top \phi(\mathbf{y}) - 2\phi(\mathbf{x})^\top \phi(\mathbf{y}) \\ &= k(\mathbf{x}, \mathbf{x}) + k(\mathbf{y}, \mathbf{y}) - 2k(\mathbf{x}, \mathbf{y}). \end{aligned} \quad (7)$$

Note that for the inner-product to be properly defined, the kernel function $k(\cdot, \cdot)$ should be symmetric ($k(\mathbf{x}, \mathbf{y}) = k(\mathbf{y}, \mathbf{x})$) and positive-definite ($k(\mathbf{x}, \mathbf{y}) > 0$ for all $\mathbf{x}, \mathbf{y} \neq \mathbf{0}$).

Besides computational efficiency, kernel methods have gained their popularity in learning also for other advantages including the existence of a wide range of kernels and their capability of dealing with infinite-dimensional feature spaces. Consider the Gaussian kernel as an example. Given two data samples $\mathbf{x}, \mathbf{y} \in \mathbb{R}$, the Gaussian kernel $k(\mathbf{x}, \mathbf{y}) = \exp \left\{ -\frac{1}{2\sigma^2} \|\mathbf{x} - \mathbf{y}\|^2 \right\}$ can be evaluated. The kernel expression implicitly defines an *infinite-dimensional* feature space induced by the following mapping:

$$\phi(\mathbf{x}) = \exp \left\{ -x^2 / 2\sigma^2 \right\} \left[1, \sqrt{\frac{1}{1! \sigma^2}} x, \dots, \sqrt{\frac{1}{n! \sigma^{2n}}} x^n, \dots \right]^\top. \quad (8)$$

2) *Grassmannian Kernel and Learning*: Learning from data sets with elements being subspaces (e.g., image features or motions) has motivated the development of the Grassmann kernel methods. Simply by defining kernel functions on the Grassmann manifold $k(\cdot, \cdot) : \mathcal{G}(n, k) \times \mathcal{G}(n, k) \rightarrow \mathbb{R}^*$ and kernel replacement, classic kernelized learning algorithms in the Euclidean space can be readily migrated onto the Grassmann manifold. The key property distinguishing a Grassmann kernel from others is that the kernel function must be invariant to the choice of specific basis in subspace data samples. In other words, given two points \mathbf{X}, \mathbf{Y} on some Grassmann manifold, the Grassmann kernel $k(\mathbf{X}, \mathbf{Y}) = k(\mathbf{X}\mathbf{U}, \mathbf{Y}\mathbf{V})$ for any $\mathbf{U}, \mathbf{V} \in \mathbf{O}(O)$. Two commonly used Grassmann kernels are the Binet-Cauchy kernel and the projection kernel given Table III. Similar to Euclidean kernels, the sum, product and composition of Grassmannian kernels also result in valid Grassmannian kernels. A detailed treatment of Grassmannian kernels can be found in e.g., [34].

The general framework of applying a Grassmann kernel method in learning from Grassmannian data is shown in Fig. 3. Raw data such as an image set is usually transformed to

Metric	Principal Angle Formulation	Matrix Formulation	Kernel
Arc Length d	$(\sum_{i=1}^k \theta_i^2)^{1/2}$	–	–
Fubini-Study d_{FS}	–	$\arccos \det \mathbf{X}^\top \mathbf{Y} $	–
Chordal d_C	$2 \left(\sum_{i=1}^k \sin^2 \frac{\theta_i}{2} \right)^{1/2}$ $= \sqrt{2} \left(k - \sum_{i=1}^k \cos \theta_i \right)^{1/2}$	$\ \mathbf{X}\mathbf{U} - \mathbf{Y}\mathbf{V}\ _F$ $= \sqrt{2} \left(k - \text{tr}((\mathbf{X}^\top \mathbf{Y} \mathbf{Y}^\top \mathbf{X})^{1/2}) \right)^{1/2}$	–
Projection d_P	$(\sum_{i=1}^k \sin^2 \theta_i)^{1/2}$	$\ \mathbf{X}\mathbf{X}^\top - \mathbf{Y}\mathbf{Y}^\top\ _F$	$\ \mathbf{X}^\top \mathbf{Y}\ _F^2$
Binet-Cauchy d_{BC}	$(1 - \prod_{i=1}^k \cos^2 \theta_i)^{1/2}$	–	$\det(\mathbf{X}^\top \mathbf{Y})^2$

TABLE III: Several common distance measures between two points \mathbf{X} and \mathbf{Y} on the Grassmann manifold where $\{\theta_i\}_{i=1}^k$ are principal angles between \mathbf{X} and \mathbf{Y} .

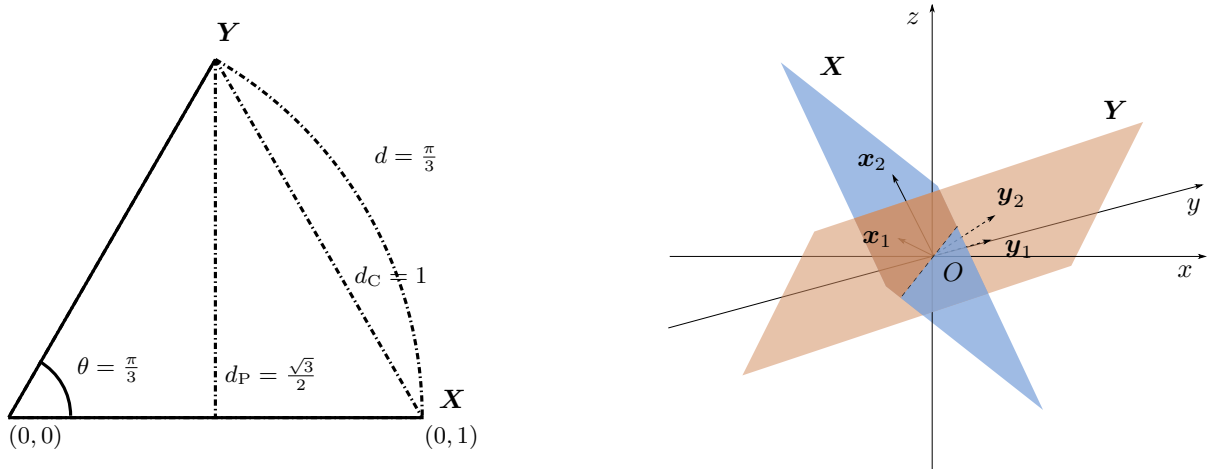
Example 1 (Subspace distances) Two concrete examples of computing distances between two points on a Grassmann manifold are given as follows.

♠ **Left:** As a simple example, consider two points $\mathbf{X} = [1 \ 0]^\top$ and $\mathbf{Y} = [\frac{1}{2} \ \frac{\sqrt{3}}{2}]^\top$ on the Grassmannian $\mathcal{G}(2, 1)$. They have only a single principal angle of $\frac{\pi}{3}$. Based on Table III and illustrated in Fig. 1, the arc length between \mathbf{X} and \mathbf{Y} is the length of the geodesic joining the points, namely $d = \frac{\pi}{3}$; the chordal distance is the chord joining them, computed as $d_C = 1$; the Projection distance is the length of the projection from \mathbf{X} to \mathbf{Y} is $d_P = \frac{\sqrt{3}}{2}$.

♠ **Right:** As a more general example, consider

$$\mathbf{X} = \begin{bmatrix} -\frac{\sqrt{2}}{2} & -\frac{\sqrt{2}}{4} \\ \frac{\sqrt{2}}{2} & \frac{\sqrt{2}}{4} \\ 0 & \frac{\sqrt{3}}{2} \end{bmatrix}, \quad \mathbf{Y} = \begin{bmatrix} 0 & \frac{\sqrt{2}}{2} \\ 1 & 0 \\ 0 & \frac{\sqrt{2}}{2} \end{bmatrix}$$

as two points on the Grassmannian $\mathcal{G}(3, 2)$. From the SVD of $\mathbf{X}^\top \mathbf{Y}$, the singular values are computed as 1.0 and 0.079. It follows from the results and Section II-B that the principal angles between \mathbf{X} and \mathbf{Y} are $\theta_1 = 0$, $\theta_2 = \arccos(0.07945931) \approx 85.44$ deg. Using Table III, different subspace distances between the points are computed as $d(\mathbf{X}, \mathbf{Y}) \approx 1.491253$, $d_{FS}(\mathbf{X}, \mathbf{Y}) \approx 1.491253$, $d_C(\mathbf{X}, \mathbf{Y}) \approx 1.356864$, $d_P(\mathbf{X}, \mathbf{Y}) \approx 0.996838$ and $d_{BC}(\mathbf{X}, \mathbf{Y}) \approx 0.996838$, which confirm the relation in (6).



Example: Geometric illustrations of subspace distance measures.

subspace features or Grassmannian representations using, for example, *principle component analysis* (PCA). By choosing a specific Grassmannian kernel function, the Grassmannian data can be fed into a kernelized learning algorithm such as classification based on support vector machine or linear

discriminant analysis. We will revisit Grassmann kernelized learning in the discussion of linear discriminant analysis in Section III-A and in deep transfer learning in Section IV-A.

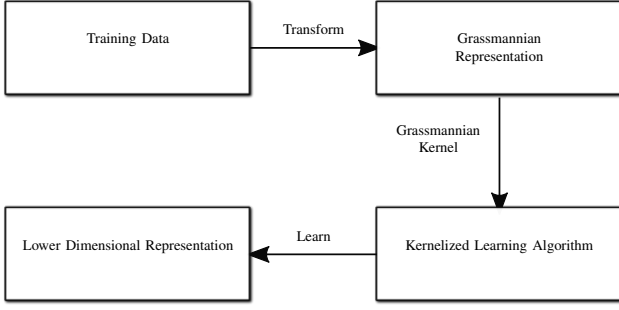


Fig. 3: General framework for Grassmannian kernelized learning.

G. Optimization on Grassmann Manifolds

Grassmannian kernel methods provide a tool for solving the class of problems involving Grassmannian data, or called Grassmann kernelized learning. There also exists another class of problems that involve optimizing variables under specific structural constraints such as sparsity or low rank in the context of matrix completion. They can be often cast as optimization problems on the Grassmann manifold, which has the typical form in (9) or its equivalence in (10). Solving such a problem represents a search for a subspace or orthogonality-constrained optimization. One example is low-rank matrix completion in Section III-C where the goal is to find a subspace that is consistent with the observed entries. Another example is the method of sample geodesic flow method for transfer learning in Section IV-A, which yields a subspace where data appears most discriminative.

Grassmann optimization problem are usually solved using is gradient-based methods such as steepest or conjugate gradient descent on the Grassmann manifold. Compared with their Euclidean-space counterparts, the key feature of such methods is the computation of a gradient on the Grassmannian manifold using the formula in (3). As discussed earlier, the gradient computation using (3) has low complexity which first evaluates the “Euclidean gradient” and then projects it onto the Grassmannian manifold to obtain the Grassmannian gradient. In practice, software packages such as ManOpt [29] are available for Grassmann gradient computation. In addition, there exist problem-specific methods for Grassmannian optimization such as convex relaxation in the sparse spectral clustering. We will apply Grassmannian optimization methods to sparse and low-rank representation learning in Section III-C and deep learning in Section IV-B.

$$\begin{aligned} \min \quad & f(\mathbf{X}), \\ \text{s.t.} \quad & \mathbf{X} \in \mathcal{G}(n, k). \end{aligned} \quad (9)$$

$$\begin{aligned} \min \quad & f(\mathbf{X}), \\ \text{s.t.} \quad & f(\mathbf{X}) = f(\mathbf{X}\mathbf{S}), \\ \text{where} \quad & \mathbf{X} \in \mathbb{R}^{n \times k}, \mathbf{S} \in \mathbf{O}(k). \end{aligned} \quad (10)$$

In summary, Grassmannian kernelized methods and Grassmannian optimization are two problem-solving paradigms

targeting two different types of problems in Grassmannian learning. Their main differences are summarized in Table IV.

Paradigm	Input Data	Optimization Domain
Grassmannian Kernel Methods	Grassmannian	RKHS
Grassmannian Optimization	General	Grassmannian

TABLE IV: Comparison between two learning paradigms: Grassmannian kernel methods and Grassmannian optimization.

III. SHALLOW GRASSMANNIAN LEARNING

This section is devoted to shallow Grassmannian learning methods, where Grassmann manifolds provide a tool for non-linear dimensionality reduction. In this section, we review several applications of shallow Grassmannian learning, including discriminant analysis in Section III-A, high-dimensional data clustering in Section III-B, and low-rank matrix completion in Section III-C. The problems share a common theme of dimensionality reduction. However, their goals in representation differ. Discriminant analysis seeks a low-dimensional subspace where data are most discriminative; high-dimensional data clustering and low-rank matrix completion attempt to learn sparse and low-rank representations. Inline with traditional dimensionality-reduction techniques that directly operate on Euclidean data, with proper notion of Grassmann kernels and distance measures as introduced in Section II, problems involving subspace data or operations on Grassmann manifolds may be made tractable or tackled more efficiently without sacrificing the geometric intuitions. For a more comprehensive and in-depth treatment of the topics, readers are referred to [35, 36].

A. Grassmann Discriminant Analysis

GDA builds on *linear discriminant analysis* (LDA). The latter is a class of supervised learning algorithms for classification based on identifying a latent subspace in which the data are most discriminative, meaning that similar data samples are close but distant from dissimilar samples [37]. The mathematical principle of LDA is described as follows. To this end, let N , C , N_c , $\boldsymbol{\mu}$, $\boldsymbol{\mu}_c$, \mathbf{x}_i denote the dataset size, number of data classes, c -th class size, population mean, class mean and the i -th data sample. Considering class c , the *intra-class covariance* with respect to the class mean $\boldsymbol{\mu}_c$ is

$$\mathbf{S}_w = \frac{1}{N} \sum_{c=1}^C \sum_{i: y_i=c} (\mathbf{x}_i - \boldsymbol{\mu}_c)(\mathbf{x}_i - \boldsymbol{\mu}_c)^\top, \quad (11)$$

while the *inter-class covariance* is defined in terms of population and class means as

$$\mathbf{S}_b = \frac{1}{N} \sum_{c=1}^C N_c (\boldsymbol{\mu}_c - \boldsymbol{\mu})(\boldsymbol{\mu}_c - \boldsymbol{\mu})^\top. \quad (12)$$

Then finding the latent discriminant subspace can be translated into the concrete problem of finding a low-dimensional subspace, denoted as $\boldsymbol{\alpha}^\top$, in which the projected inter-class

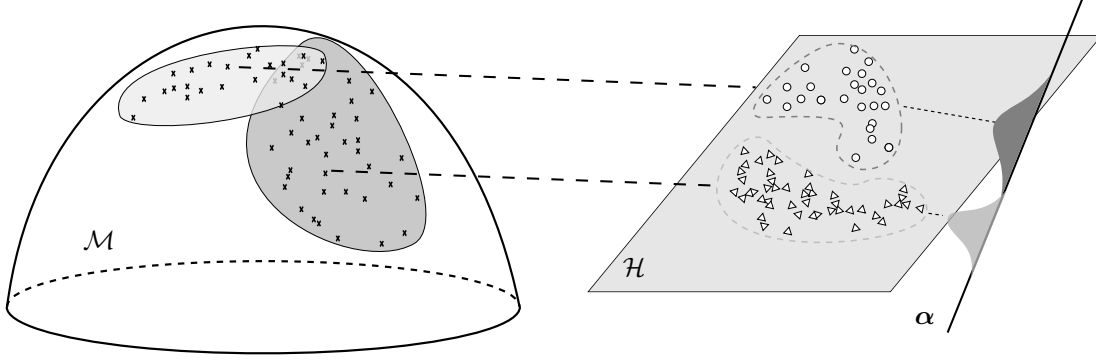


Fig. 4: Illustration of kernelized GDA: Kernelized GDA firstly projects data on the Grassmann manifold \mathcal{M} to some RKHS \mathcal{H} constructed from a specific Grassmannian kernel, and then performs discriminant analysis in this space.

covariance is maximized and the projected intra-class covariance minimized. The two objectives can be combined, leading to the optimization of the Rayleigh quotient

$$f(\alpha) = \frac{\alpha^\top S_b \alpha}{\alpha^\top S_w \alpha}. \quad (13)$$

Based on the covariance definition in (11) and (12), LDA targets generic data distributed in the linear Euclidean space. For applications such as image-set classification or action recognition, direct extension of LDA to handle Grassmannian data, meaning data on a nonlinear Grassmann manifold, is not trivial. First of all, how should mean and variance be defined on the manifold? As the manifold is nonlinear and data similarity is measured using subspace distances, the arithmetic in (12) and (11) are no longer meaningful and need be modified. There do exist a handful of notions of mean on the Grassmann manifold such as Procrustes mean and Karcher mean [33]. Their computation, however, typically involves solving a Grassmannian-optimization problem by a iterative Grassmannian-gradient method. As first proposed in [38], a more efficient and systematic approach for GDA is to develop kernelized discriminant analysis and leverage Grassmann kernels introduced in Section II-F.

The essence of the Grassmannian kernel approach is to define the Grassmann counterparts of the covariance matrices in (12) and (11) in terms of a kernel matrix. Let \mathbf{K} denote such a matrix where the element $K_{ij} = k(\mathbf{X}_i, \mathbf{X}_j)$ for some Grassmannian kernel function $k(\cdot, \cdot)$ defined in Section II-F and two Grassmann data samples \mathbf{X}_i and \mathbf{X}_j . Define $[\frac{1}{N}]$ as an $N \times N$ matrix with each entry being $1/N$ and \mathbf{V} as an N by N block diagonal matrix with the i -th block being $[\frac{1}{N_C}]$, the intra-class and inter-class covariance matrices for GDA can be written as $\mathbf{S}_w = \mathbf{K}(\mathbf{I}_N - \mathbf{V})\mathbf{K}$ and $\mathbf{S}_b = \mathbf{K}(\mathbf{V} - [\frac{1}{N}])\mathbf{K}$ [3]. The definitions allow the quotient minimization in (13) to be modified to a kernelized version for GDA as [3]

$$f(\alpha) = \frac{\alpha^\top \mathbf{K}(\mathbf{V} - [\frac{1}{N}])\mathbf{K}\alpha}{\alpha^\top (\mathbf{K}(\mathbf{I}_N - \mathbf{V})\mathbf{K} + \epsilon^2 \mathbf{I}_N)\alpha}, \quad (14)$$

where $\epsilon^2 \mathbf{I}$ is optional and added for numerical robustness in practice.

The GDA is an exemplar application of the general kernel methods on the Grassmann manifold discussed in Section

II-F. The learning process is illustrated in Fig. 4 for a dataset consisting of two classes. The Grassmannian data (obtained by preprocessing the raw data, for example) can be viewed as being projected to an RKHS implicitly defined by the kernel function where data discriminative properties are retained. Thereby, LDA algorithms can be applied in this RKHS governed by a distance measure induced by the kernel. This yields a low-dimensional subspace where a classifier for Grassmannian data can be trained and subsequently applied to label future new data. By substituting proper Grassmannian kernels, learning on the Grassmann manifold can be built on top of the Euclidean kernelized learning algorithm with ease. We will revisit the GDA approach in the context of image classification in Section V.

B. High-Dimensional Data Clustering

In this subsection, we will examine how the classic topic of high-dimensional data clustering can be cast as a Grassmannian optimization problem. **Spectral clustering** is a popular technique for dimensionality reduction in clustering high-dimensional data, which has been adopted in many signal processing applications for its simplicity and performance [39, 40, 41]. The technique derives its name from the operation on the spectrum (i.e., the eigenvalues) of the Laplacian matrix of the affinity matrix specifying pairwise similarity of data samples. The operations of spectral clustering are illustrated in Fig. 5 and elaborated as follows.

Given a set of data samples $\{x_i\}_{i=1}^N$ from k clusters, Step 1 is to construct an affinity matrix $\mathbf{W} \in \mathbb{R}^{N \times N}$ that contains pairwise sample similarity using the distance measure $d(\cdot, \cdot)$ in the original data space. For example, \mathbf{W} may be constructed using a Gaussian kernel such that its (i, j) -th element $W_{ij} = \exp\{-\frac{1}{2\sigma^2}d^2(x_i, x_j)\}$. The construction of such a matrix, called *similarity encoding*, provides a convenient overview of the similarity heat map for the considered dataset as illustrated in Fig. 5 and Example 2 and thereby facilitates the subsequent data clustering.

As Step 2, the similarity “heat-map” can be enhanced by constructing the so-called Laplacian matrix of \mathbf{W} via $\mathbf{L} = \mathbf{D} - \mathbf{W}$ for unnormalized Laplacian and $\mathbf{L} = \mathbf{I} - \mathbf{D}^{-1/2}\mathbf{W}\mathbf{D}^{-1/2}$ for normalized one, where $\mathbf{D} \in \mathbb{R}^{N \times N}$ is a diagonal matrix with diagonal entries being the sum of each

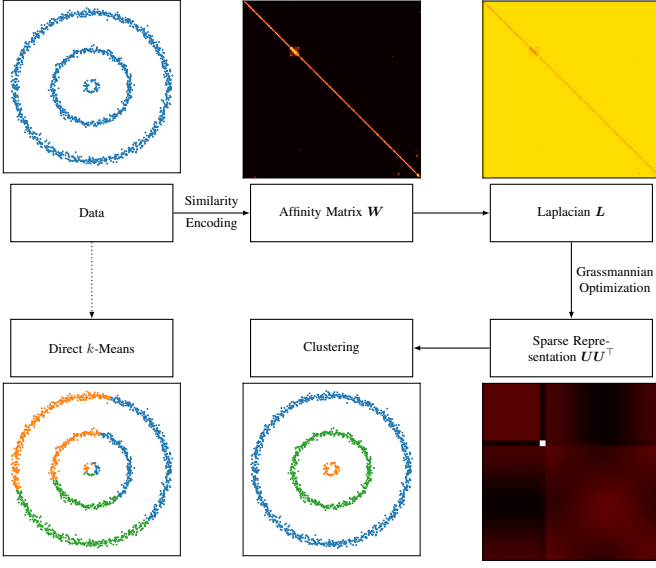


Fig. 5: Operations and example of spectral clustering. The three-ring data where each cluster has a ring shape, affinity matrix W , unnormalized Laplacian L (in logarithmic scale), sparse representation UU^T and the final result. The three diagonal blocks in the W , L , and UU^T heat map (bottom right) correspond to three clusters. Noted direct clustering using k -means is ineffective.

row in W [42]. The Laplacian matrix L is a notation from graph theory and widely used in computer-vision tasks such as blob and edge detection. Roughly speaking, it captures the difference between a specific data sample and the average value of those which are close to it. Compared with W , a local measure of similarity, the Laplacian L takes the global structure of the dataset into consideration and thus is expected to achieve a better clustering performance.

Step 3 is to eigen-decompose L and extract data's low-dimension representations for subsequent clustering. The k eigenvectors of L corresponding to the k smallest eigenvalues, denoted by $U \in \mathbb{R}^{N \times k}$, can be viewed as a low-dimensional representation that provides the key structural information of the dataset. This allows each data sample to be represented by a k -dimensional row vector of U . It is expected that in this extracted low-dimensional feature space. The data clustering structure can be better revealed, thus leading to both performance boost and complexity reduction for clustering in the subspace (using a standard algorithm such as k -means) compared with that in the original high-dimensional data space. A simple example is given in Fig. 5 where clustering in the feature space is effective while that in the original data space is not.

Building on the above basic technique, **sparse spectral clustering** attempts to improve the accuracy in representation by exploiting the sparse structure in the affinity matrix W [43]. In the ideal case where a dataset is comprised of well separated clusters, data similarity should be local, i.e., data from the same cluster are similar to each other but dissimilar to those from other clusters. Consequently, the affinity matrix W should be block diagonal (with each block correspond to

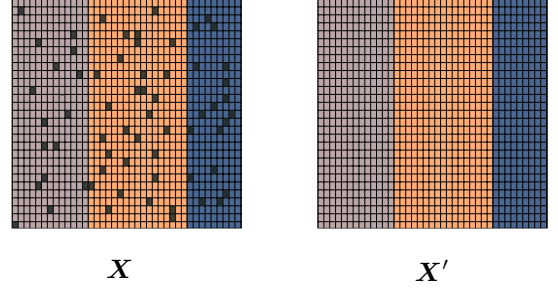


Fig. 6: Illustration of low-rank matrix completion.

one cluster) and thus exhibits a sparse structure [44]. It is further argued in [43] that the low-dimensional representation UU^T defined earlier should be also sparse. Specifically, each row of U may be a “one-shot encoded” representation of the corresponding data point with only a “1” at the location whose index identifies the corresponding cluster and “0”s at other locations. It follows that samples with identical encoded representations belong to the same cluster. Furthermore, U is of rank k and also sparse since there are many zeros entries that do not contribute to its rank. Given the sparsity, sparse spectral clustering can be formulated as an optimization problem for minimizing the discrepancy between the Laplacian matrix L of W and its low-dimensional representation UU^T as measured by their inner-product plus a penalty term $\beta \|UU^T\|_0$ that counts the number of nonzero elements and thus imposes a sparsity constraint. Since optimization over L_0 norm is known to be NP-hard, a common relaxation is to use the L_1 norm instead [43]. This yields the following problem of sparse spectral clustering:

$$\begin{aligned} \min_U \quad & f(U) = \langle UU^T, L \rangle + \beta \|UU^T\|_1 \\ \text{s.t.} \quad & U^T U = I_k. \end{aligned} \quad (15)$$

Due to the orthogonality constraint on U , we can cast the problem in (15) into a **Grassmannian optimization** problem based on the framework discussed in Section II:

$$\begin{aligned} \min_U \quad & f(U) = \langle UU^T, L \rangle + \beta \|UU^T\|_1 \\ \text{s.t.} \quad & U \in \mathcal{G}(n, k). \end{aligned} \quad (16)$$

The optimization in (16) attempts to find a desired subspace but not a specific basis, making it a suitable application of Grassmannian optimization. To verify this fact, one can observe that the objective function in (16) is invariant to any right rotation of the variable U since $URR^T U^T = UU^T$ with $R \in \mathcal{O}(k)$ being a $k \times k$ rotation (unitary) matrix. It follows that the problem in (16) can be solved using the procedures for Grassmannian optimization described in Section II. Based on the resultant low-dimensional representation of the data samples in U , different clusters can be identified. The classical example of three rings is shown in Example 2 to illustrate the power of Grassmannian-aided sparse representation learning.

C. Low-Rank Matrix Completion

Another classic problem in low-rank representation learning is **low-rank matrix completion**, namely filling in the missing

Example 2 (Sparse Spectral Clustering of Three-Ring Dataset) We consider an three-ring dataset in \mathbb{R}^2 with $N = 1550$ data samples forming $k = 3$ ring clusters. The clustering problem in (16) is solved using the method of steepest descent on the Grassmannian with the penalty $\beta = 0.01$ and varying $\sigma \in \{0.1, 1, 1.6, 3, 5\}$, the bandwidth in the Gaussian kernel used for constructing \mathbf{W} . The rows in Fig. 7 are the heat map of $\mathbf{U}\mathbf{U}^\top$, the embedding of \mathbf{U} in \mathbb{R}^3 , and the clustering results and the columns different values of σ . The structural information can be inferred from the heat maps. For example, starting at $\sigma = 1.6$, one can observe three diagonal blocks in the heat map, indicating the existence of three clusters. The parameter σ has a significant effect on the performance, governing how the Grassmannian optimization can disentangle data in the low dimensional latent space determined by \mathbf{U} . For small σ , the affinities between data samples are reduced; data samples are pushed away from each other and appear isolated. Increasing σ amplifies similarity and pulls data samples together, resulting in parallel circles on the sphere in the latent space. Undesirable clustering results arises from either too small or too large σ is. With a properly chosen σ (1.6 in this case), all three clusters are concentrated in separate small regions in the latent space generated by \mathbf{U} (second row in Fig. 7). Consequently, data rings are desirably clustered as marked in different colours (bottom row in Fig. 7). Note that in practice, the optimal value of σ can be found by line search.

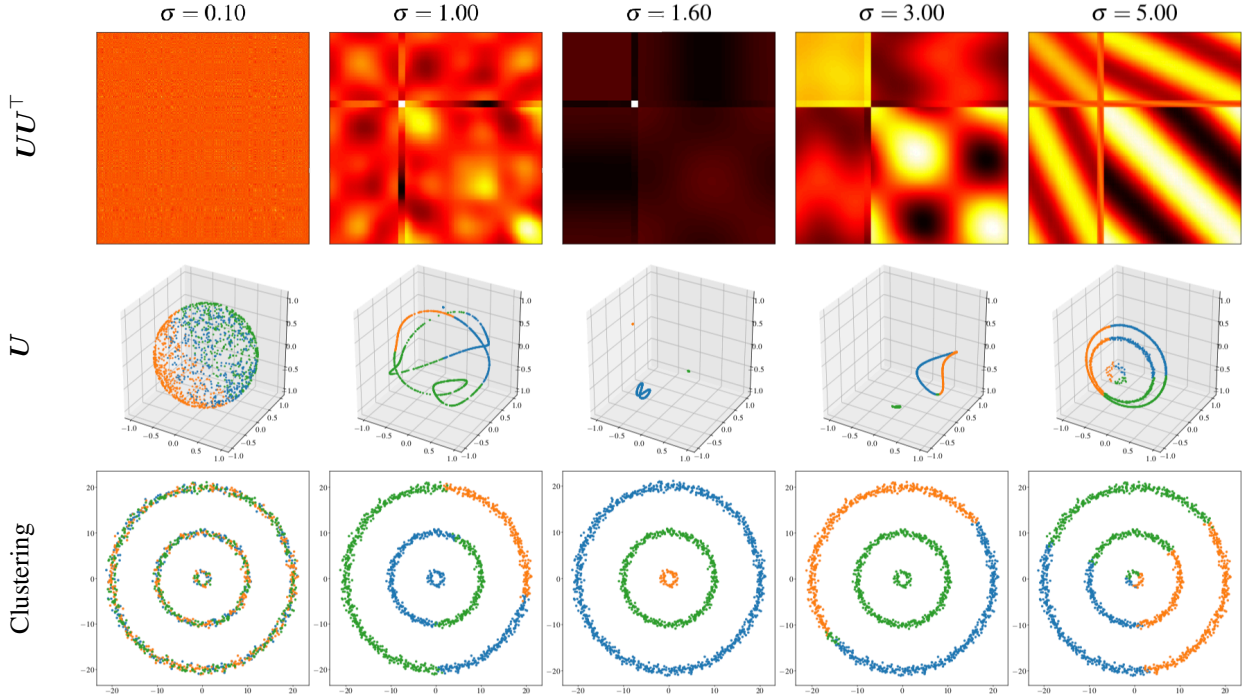


Fig. 7: Example of sparse spectral clustering via Grassmann optimization.

entries of a given matrix. Though the general problem is ill-posed, it is tractable under the assumption that the matrix to be filled is low-rank. We give an illustration of the problem in Fig. 6. The incomplete matrix \mathbf{X} has a rank of 3 as characterized by three one-rank blocks in different colours. The black rectangles correspond to the missing entries, which can be filled in based on consistency with the observed entries. Thereby, the complete matrix \mathbf{X}' can be reconstructed from the partially observed matrix \mathbf{X} .

Mathematically, the problem of low-rank matrix completion can be formulated as follows. Consider a matrix $\mathbf{X} \in \mathbb{R}^{n \times k}$ with $k \leq n$ and a constraint on its rank $r \leq \min\{n, k\}$. Let us define an indicator matrix $\Omega_{\mathbf{X}}$ for observed entries such that $\Omega_{ij} = 1$ if \mathbf{X}_{ij} is observed and 0 otherwise. The aim is to find a low-rank reconstruction of \mathbf{X} that is consistent with the observed entries in \mathbf{X} . More formally, let \mathcal{P}_{Ω} denote a mapping that maps all unobserved entries to 0 and keeps the

observed entries:

$$\mathcal{P}_{\Omega} : \mathbf{X} \mapsto \mathbf{X}_{\Omega} = \begin{cases} \mathbf{X}_{ij}, & \Omega_{ij} = 1, \\ 0, & \text{otherwise.} \end{cases} \quad (17)$$

The matrix-completion problem seeks a matrix $\mathbf{X}' \in \mathbb{R}^{n \times k}$, such that $\text{rank}(\mathbf{X}') = r$ and $\mathcal{P}_{\Omega}(\mathbf{X}') = \mathcal{P}_{\Omega}(\mathbf{X}) = \mathbf{X}_{\Omega}$. This problem is usually reformulated as a *subspace identification* problem that searches for the column space of the desired matrix \mathbf{X} , denoted as \mathbf{U} , that is consistent with that of the observed matrix \mathbf{X}_{Ω} by finding the minimum Frobenius-norm based distance $f_F(\mathbf{U}, \mathbf{X}_{\Omega})$:

$$\begin{aligned} \text{solve } f_F(\mathbf{U}, \mathbf{X}_{\Omega}) &= \min_{\mathbf{W} \in \mathbb{R}^{k \times r}} \left\| \mathbf{X}_{\Omega} - \mathcal{P}_{\Omega}(\mathbf{U}\mathbf{W}^\top) \right\|_F^2 = 0, \\ \text{s.t. } \mathbf{U}^\top \mathbf{U} &= \mathbf{I}_n, \end{aligned} \quad (18)$$

where the right-multiplication of \mathbf{W} on \mathbf{U} amounts to a proper transformation to align \mathbf{X} with the coordinates of \mathbf{X}_{Ω} within

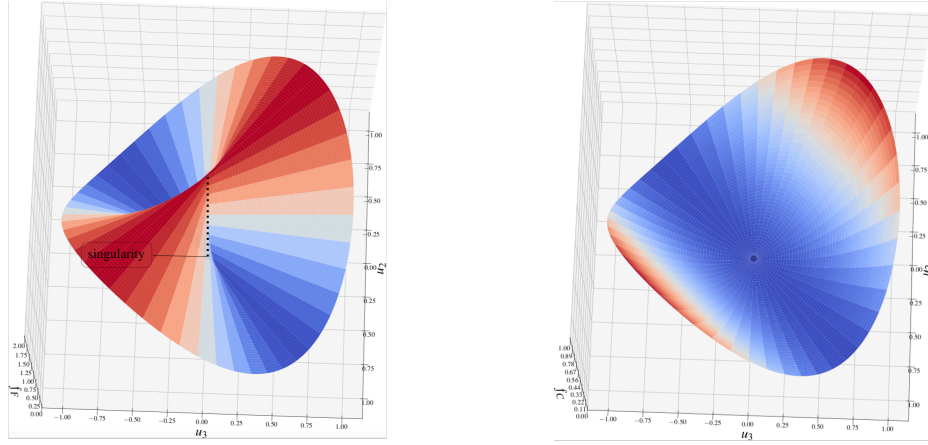


Fig. 8: Objective function profiles for (left) Frobenius-distance formulation and (right) projection-distance formulation.

the subspace U . It is found in [8] that the use of Frobenius norm in (18) introduces singularities that may cause difficulty in applying the gradient based methods to search for the global minimum [8].

This issue can be fixed by recasting the the problem in (18) as a **Grassmannian optimization problem** that leverages the geometry of the original formulation, namely that the optimization variable U is more properly modelled as an element on some Grassmann manifold rather than an ordinary orthonormal matrix. The reason is that the minimization over W makes the objective function $f_F(U, X_\Omega)$ invariant to rotation of U , which makes the problem in (18) defined on the Grassmannian rather than that in (15) on the Stiefel manifold. For the reformulation, a required step is to design a proper measure of the subspace-distance between the low-rank representation U and the partially observed matrix X_Ω , denoted as $f_S(U, X_\Omega)$, such that the measure is everywhere continuous without any singularity. This facilitates the solving of the following reformulated Grassmannian-optimization problem

$$\begin{aligned} \min \quad & f_S(U, X_\Omega), \\ \text{s.t.} \quad & U \in \mathcal{G}(n, k) \end{aligned} \quad (19)$$

using the gradient based method discussed in Section II-G.

One such design is proposed in [8] and briefly described as follows. Let x_i denote the i -th of a total of n rows of the partially observed matrix X_Ω where the missing entries are filled with zeros. A matrix B_i is then constructed by cascading the column vector x_i and a set of basis vectors $\{e_j\}$, each of which has a “1” at the j -th entry and 0s elsewhere:

$$B_i = [x_i, e_j, e_{j'}, \dots] \quad (20)$$

where $\{e_j\}$ are chosen such that the rows of B_i corresponding to the missing entries in x_i each has a “1” entry and zeros elsewhere. Then an objective function enabling Grassmannian optimization is designed as follows:

$$f_P(U; X_\Omega) = \sum_{i=1}^n d_P(B_i, X_\Omega), \quad (21)$$

where $d_P(A, B) = 1 - \lambda_{\max}(A^T B)$ is the projection distance, a subspace distance measure, between two matrices A and B

and $\lambda_{\max}(\cdot)$ gives the maximum singular value of its argument. As illustrated in Fig. 8, the new objective function $f_P(U; X_\Omega)$ based on subspace distance has a smooth profile while that of the original one based on F-norm has singularities causing difficulty in conducting gradient descent algorithm.

IV. DEEP GRASSMANNIAN LEARNING

The revival of artificial neural networks and deep learning has achieved unprecedented success in a wide spectrum of applications including computer vision, natural language processing and artificial intelligence [16]. Recently, researchers started to develop geometric techniques such as geodesic convolution [19] and matrix back-propagation [45] for fully unleashing the potential of deep neural networks in solving problems having embedded geometric structures [17]. In the same vein, one may ask how Grassmann manifolds can be incorporated into deep learning to streamline its operation or improve its performance in certain applications, leading to deep Grassmannian learning. In this section, two specific areas of deep Grassmannian learning are introduced, namely visual domain adaptation (or transfer learning) in Section IV-A and the construction of deep neural networks for Grassmannian inputs or outputs Section IV-B.

A. Transfer Learning

Transfer learning refers to the task of generalizing the knowledge of a model learned in one domain (source) to another domain (target) e.g., from handwriting recognition to street-sign recognition, or from natural language processing in one language to that in another. Currently, the most prevalent methods lie in one of three categories: [46]

- 1) (Dimensionality Reduction) The methods are based on the assumption that datasets from different domain share similar representations in a certain latent feature space that can be recovered using a dimensionality reduction technique;
- 2) (Data Augmentation) The principle of these methods (such as geodesic-flow methods discussed in the sequel) is to intelligently mix the datasets from the source

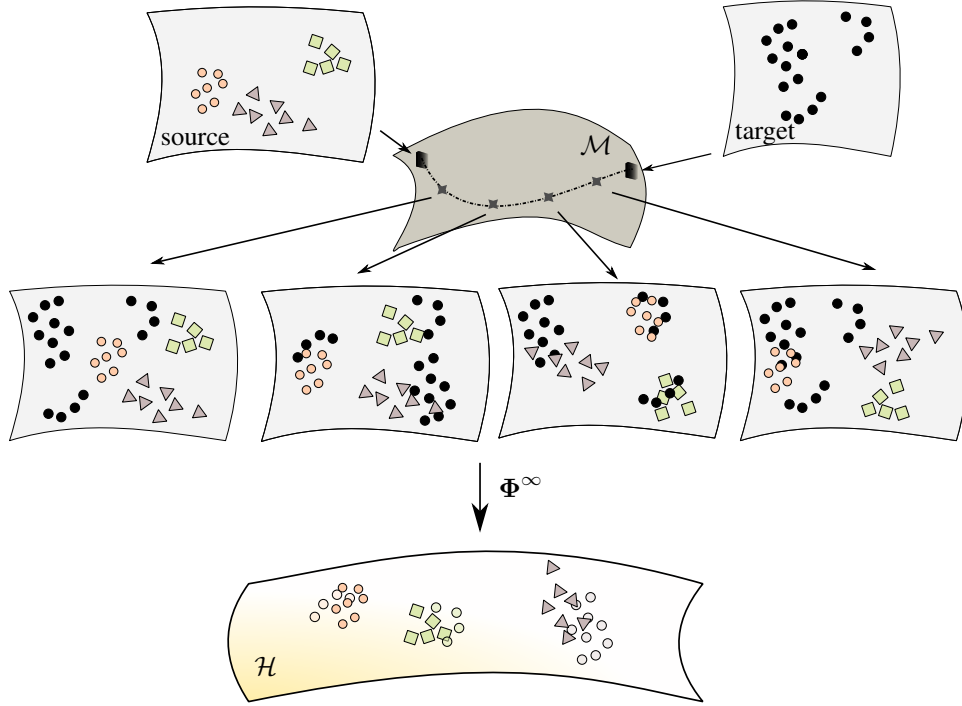


Fig. 9: Geodesic-sampling based transfer learning.

and target domains such that the latent feature space mentioned earlier becomes not only explicit but even dominant, allowing its extraction.

- 3) (Deep Learning) The methods involves the deployment of deep neural networks in transfer learning and may not be mutually exclusive with previous two types.

This subsection focuses on a key topic of transfer learning, namely **visual domain adaptation**, and its relevance to Grassmannian learning. One example is using the model for recognizing objects in the images on Amazon to recognize objects in the wild. To be precise, a typical task of visual domain adaptation is defined as follows. Given N labeled data samples in the source domain encompassing C classes with N_c observations in each class. Therefore, the dataset can be represented by $\{s_{c,i} : c = 1, 2, \dots, C, i = 1, 2, \dots, N_c\}$. Then (unsupervised) transfer learning aims at predicting the class labels of the observations in the target domain where data samples are unlabeled. In the remainder of this subsection, we will discuss an approach in Grassmannian deep learning for performing this task.

1) *Geodesic-Flow Methods*: The geodesic-flow methods rely on the assumption that the same class of images in two different domains may be modelled as separate points (subspaces) on a low-dimensional Grassmann manifold. An intermediate subspace on the Grassmann geodesic linking the domains may be viewed as a reasonable latent feature space for learning a common representation. Unlike many other methods inline with this philosophy [46], the geodesic-flow methods model the source and target domains as points on the Grassmann manifold. We consider two methods in the discussion: *sample geodesic flow* (SGF) [23] and *GFK* [24]. As illustrated in Fig. 9, these methods explore intermediate latent

spaces by sampling the geodesic joining the two domains. Based on the same principle, SGF and GFK differs in how the latent space is generated from the geodesic.

First, consider the SGF method that aims at seeking discrete and finite samples of the geodesic. The idea is illustrated in the upper half of Fig. 9. By traversing along the geodesic, the distributions of features (or latent representations) from two domains may be most similar at some location, where the classes in the source domain can be identified leveraging the classifier from the source domain. Mathematically, the geodesic from the source domain X_s to the target domain X_t , denoted as Φ , can be constructed using the CS decomposition (5) introduced in Section II-D. Let the tangent at X_s on the Grassmannian be denoted as Δ . The geodesic can be written as

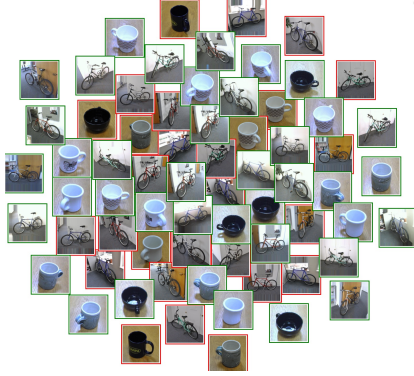
$$\Phi(t) = X_s U_1 \Gamma(t) V^\top - \Delta U_2 \Sigma(t) V^\top. \quad (22)$$

Given the geodesic, SGF samples a finite number of points on the geodesic, $\{\Phi(t_n)\}$, and uses the one that performs the best (based on e.g., a line search) to transfer the source classifier to label the target-domain data samples.

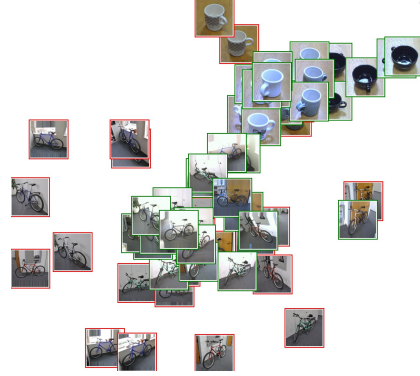
Next, consider the GFK method. By exploiting the kernel method, GFK provides an elegant way of data augmentation (integrating datasets from source and target domains) by making use of all intermediate subspaces across the geodesic. The mathematical principle of GFK is to introduce a latent RKHS by integrating over the geodesic and thereby constructing a so called *geodesic-flow kernel* as illustrated in the lower half of Fig. 9. Specifically, the geodesic-flow kernel matrix K can be computed by

$$x_i^\top K x_j = \int_0^1 (\Phi(t)^\top x_i)^\top (\Phi(t)^\top x_j) dt. \quad (23)$$

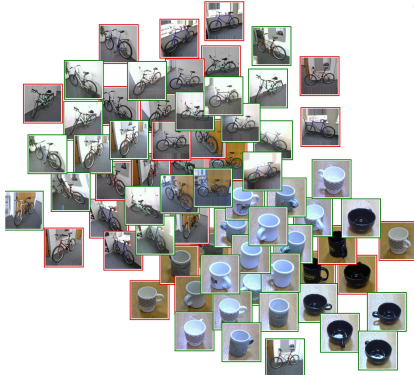
Experiment 1 (Transfer Learning Using SGF/GFK) The source and target domains are `dslr` (red framed-boxes) and `webcam` (green framed-boxes) datasets from the Office dataset. Images in the two categories "bike" and "mug" are used in the experiment. The visualization relies on the classic *t-distributed stochastic embedding* (*t*-SNE) algorithm for projecting (image) data points onto the paper (\mathbb{R}^2). As the input for visualization, the image features are extracted using the well-known SURF feature extractor. The experimental results are shown in the figures below. (**Upper Left**) The original SURF feature distribution of the images show that the clusters of "bikes" and "mugs" are not differentiable. (**Upper Right**) By applying GFK, the dominant feature space is identified as shown in the subfigure. One can observe that "bikes" and "mugs" are well separated into clusters, the clusters in different domains but the same category are aligned. The results from SGF at the locations of $t = 0.4$ and $t = 0.6$ on the geodesic are shown in **Lower left** and **Lower Right**, respectively. One can observe that the $t = 0.6$ result is better than that for $t = 0.4$ and approaches the performance of GFK.



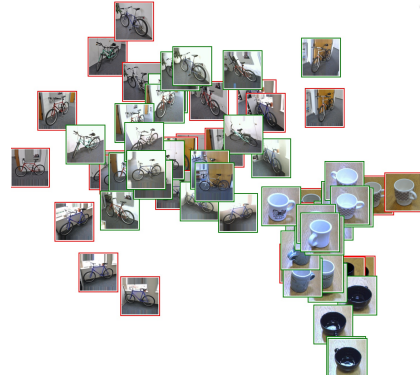
(a) Original (SURF) feature space.



(b) Feature space from GFK.



(c) Feature space from SGF with $t = 0.4$.



(d) Feature space from SGF with $t = 0.6$.

Essentially, by integrating along the geodesic to construct the flow kernel, all significant features that are discriminant in both domains are amplified and retained in the infinite-dimensional RKHS. This enables an effective knowledge transfer from the source domain to the target domain. As a result, GFK outperforms SGF.

To illustrate the effectiveness of GFK and SGF, an experiment has been carried out and the results are presented in Experiment 1.

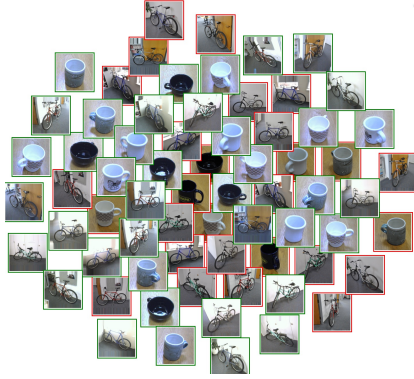
2) *Integrating Geodesic-Flow and Deep Learning*: It is widely known that the quality of features extracted from data impacts learning performance. Considering the power of deep neural networks in feature extraction, a natural and interesting question to ask is: Is it helpful to integrate the preceding geodesic-flow methods with deep neural networks? Indeed,

a geodesic-flow method can be applied on features extracted using deep neural networks to improve the transfer-learning performance. To substantiate this point, two experiments have been conducted that show significant performance improvements contributed by deep learning. The detailed results are presented in Experiments 2 and 3.

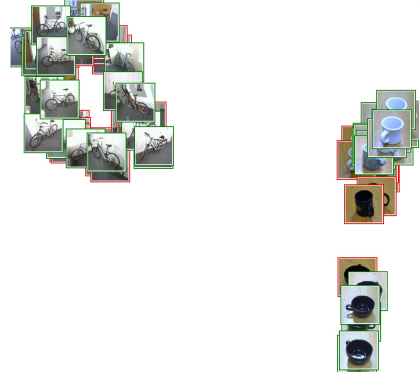
B. Deep Neural Networks on the Grassmann Manifold

In the preceding section, the simple cascading of deep neural networks for feature extraction and Grassmannian learning for domain adaption shows promising results. This suggests the direction of constructing deep neural networks that directly operate on the Grassmann manifold, targeting applications with Grassmannian input data (e.g., image sets [21]) or subspaces as output [25]. Recently, some progress has been

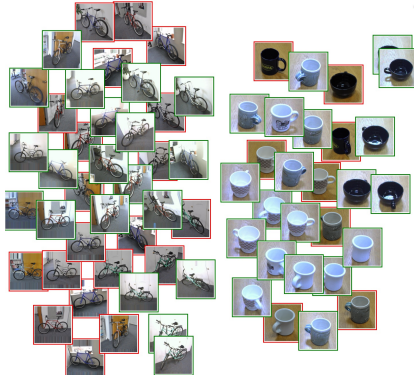
Experiment 2 (SGF/GFK with Deep Feature Extraction) Consider the settings in Experiment 1 but the features of “mug” and “bike” images are now extracted using a deep neural network instead of SURF, a shallow-learning technique. Specifically, the VGG-16 model (a 16-layer neural network) [47] pretrained on the large-scale image database called *ImageNet* [48] is applied to perform feature extraction, which generates 4096-dimensional features for each image. Then the features are fed into GFK/SGF transfer learning. The visualization of the results are provided in the figures below. **(Upper left)** Like the SURF features in Experiment 1, the distributions of the original features (from the second last fully-connected layer of VGG-16) cannot directly lead to the separation of “bikes” and “mugs”. **(Upper left)** Nevertheless, the application of GFK extracts a feature space where the two categories are perfectly separated and the representations in the source and target domains are well aligned. One can observe substantial performance gain of deep learning over shallow learning in Experiment 1. Similar conclusions can be drawn for SGF with $t = 0.4$ **(Lower left)** and $t = 0.6$ **(Lower right)**. Comparing GFK and SGF, the former significantly outperforms the latter in the current context of deep learning.



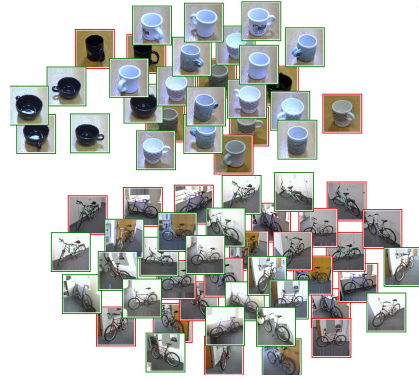
(a) Original VGG feature space.



(b) Feature space from GFK.



(c) Feature space from SGF with $t = 0.4$.



(d) Feature space from SGF with $t = 0.6$.

made in this direction. In particular, several building blocks for constructing deep neural networks on manifolds (Grassmann or general Riemann manifolds) have been developed [49, 19]. The framework of matrix back-propagation was first proposed in [45], which generalizes the conventional vector version for gradient calculation. Advanced matrix analysis tools including partial derivatives of decompositions are deployed in developing the framework. Subsequently, the framework was further developed in [49] for tackling matrices under orthogonality constraints and thus lying on the Stiefel manifolds. In this line of research, operations in the conventional vector-based neural networks such as pooling and normalization layers are redesigned for handling manifold-type data and signals. For instance, inspired by the success of convolutional layers,

the notion of geodesic convolution was proposed in [19]. Its strength lies in tasks such as establishing shape correspondence and shape retrieval in pose-recognition. Nevertheless, neural network layers thus designed cannot be directly extended to support Grassmann deep learning as most operations (either linear or nonlinear transformations) are incapable of preserving the geometry of the Grassmann manifolds. To enforce the Grassmannian constraints on the component network layers, a number of methods have been proposed which fall into one of two major approaches, namely the *intrinsic* and *extrinsic* approaches, depending on whether a method requires embedding a manifold in a higher-dimensional Euclidean space as elaborated in the sequel. We illustrate the principles and key operations for these approaches in Fig. 10. They are

Experiment 3 (Shallow vs. Deep Features) Experiment 2 demonstrates the promising performance in visual domain adaption by enhancing (Grassmann) geodesic-flow methods with deep feature extraction. Inspired by the result, a more comprehensive investigation is carried out in this experiment based on 10 image categories (instead of 2 in Experiment 2) from multiple domains A: Amazon, W: WebCam, D: DSLR and C: Caltech-256. Their different combinations create multiple transfer scenarios e.g., $A \rightarrow C$ means A is the source and C is the target domains. We compare shallow and deep feature extraction using the SURF and the VGG-16 model pretrained on the ImageNet. We trained four support vector machine (SVM) classifiers using the SURF or VGG16 features in the source domain with or without the help of GFK. Their different combinations correspond to the first four rows in Table V. We also include a model using VGG16 pretrain on the ImageNet and fine tuned in the source domain as both feature extractor and classifier in the fifth row. We report the average classification accuracies tested in the target. The results corroborate the two conclusions in Experiment 2. First, compared with the direct-transfer approach, the application of GFK is effective in adapting to domain shifts by avoiding overfitting to the source domain. Second, geodesic-flow based transfer learning based on deep features substantially outperforms all other approaches with shallow features (SURF) or direct transfer. The performance gain is largest when the domain shift is large e.g., $D \rightarrow C$.

	$A \rightarrow C$	$D \rightarrow A$	$D \rightarrow C$	$W \rightarrow A$	$W \rightarrow C$	$C \rightarrow W$
SURF+SVM	36.20 ± 2.83	30.15 ± 3.34	29.18 ± 3.01	29.55 ± 4.38	27.78 ± 3.91	22.69 ± 3.67
SURF+GFK+SVM	33.25 ± 2.91	29.25 ± 5.18	27.50 ± 2.92	24.15 ± 5.13	23.68 ± 3.78	25.50 ± 4.65
VGG+SVM	79.38 ± 2.74	75.08 ± 6.15	63.55 ± 4.55	69.55 ± 5.82	59.40 ± 4.99	78.00 ± 5.37
VGG+GFK+SVM	84.65 ± 2.28	81.68 ± 3.75	77.72 ± 3.82	76.65 ± 3.89	72.70 ± 3.90	77.62 ± 5.23
VGG	82.66	46.87	48.99	58.66	55.30	73.90

TABLE V: Unsupervised domain adaptation with shallow and deep features.

discussed in the following subsections. Before that, we remark that despite some initial progress, the field of Grassmannian deep learning is nascent field and potentially a gold mine of research opportunities.

1) *Intrinsic Grassmann Deep Learning*: There exists two methods for constructing deep neural networks that operate **intrinsically** on the Grassmann manifold. Both methods are depicted in the lower half of Fig. 10. The first is to identify points on the Grassmann manifold by projecting it to the corresponding *symmetric positive definite* (SPD) manifold via the mapping $\mathbf{X} \mapsto \mathbf{X}^\top \mathbf{X}$. As a result, the linear transformation between layers in a neural network is modified from $\mathbf{X} \mapsto \mathbf{W}^\top \mathbf{X}$ to $\mathbf{W}^\top \mathbf{X} \mathbf{W}$ for some learnable weights \mathbf{W} in the projection layer as proposed in [50]. Note that the output $\mathbf{W}^\top \mathbf{X} \mathbf{W}$ is on the SPD manifold whenever \mathbf{X} is. Thereby, the structure of the SPD manifold is preserved.

The other method based on the intrinsic approach is to design specific projection layers that preserve the manifold geometry. The so called “GrNet” (Grassmann network) proposed by [21] utilizes the QR decomposition to devise layers that output the \mathbf{Q} component of the result after some linear transformations, which in effect restricts the output to lie on some Grassmann manifold. Then conventional Euclidean loss functions can be concatenated after a projection layer and used for gradient-descent based training. The key mathematical tools in the design include the differentiation of QR and eigen decompositions for back-propagation whose details can be found in [21, 45]. The architecture of the GrNet is depicted in Fig. 11.

The initial attempts on developing customized deep neural network for Grassmannian data such as GrNet [21] or SPDNet

[50] have yielded promising performance in tasks such as video-based classification, emotion classification and activity recognition. Further investigations in this direction are necessary to fully leverage the rich literature of signal processing on Grassmann manifolds and reduce the generalization error by improving the network architecture.

2) *Extrinsic Grassmann Deep Learning*: The extrinsic approach preserves the Grassmannian geometry by projecting Grassmannian data onto the tangent space at some chosen origin as depicted in the upper half of Fig. 10. Since the tangent space is a vector space, one may deploy a neural network with regular linear layers to operate on tangent vectors. Specifically, a conventional deep neural network can be trained to learn a mapping from input data space (typically Euclidean space) to the tangent space of some Grassmann manifold. The result is then projected back on the manifold by logarithmic map (see Section II-D). This approach also enables us to generate Grassmannian outputs from Euclidean data, which is referred to as the *geodesic regression* in [25]. Methods based on the extrinsic approach have been demonstrated to be effective in learning a subspace-invariant representation of illumination spaces in images.

V. APPLICATIONS

In this section, several canonical applications of Grassmannian learning are discussed, including image-set/video based classification, wireless communications, and recommender systems.

a) *Image-set/Video Based Recognition and Classification*: Image/video based recognition or classification is a classical problem in computer vision. Prior to the resurgence of

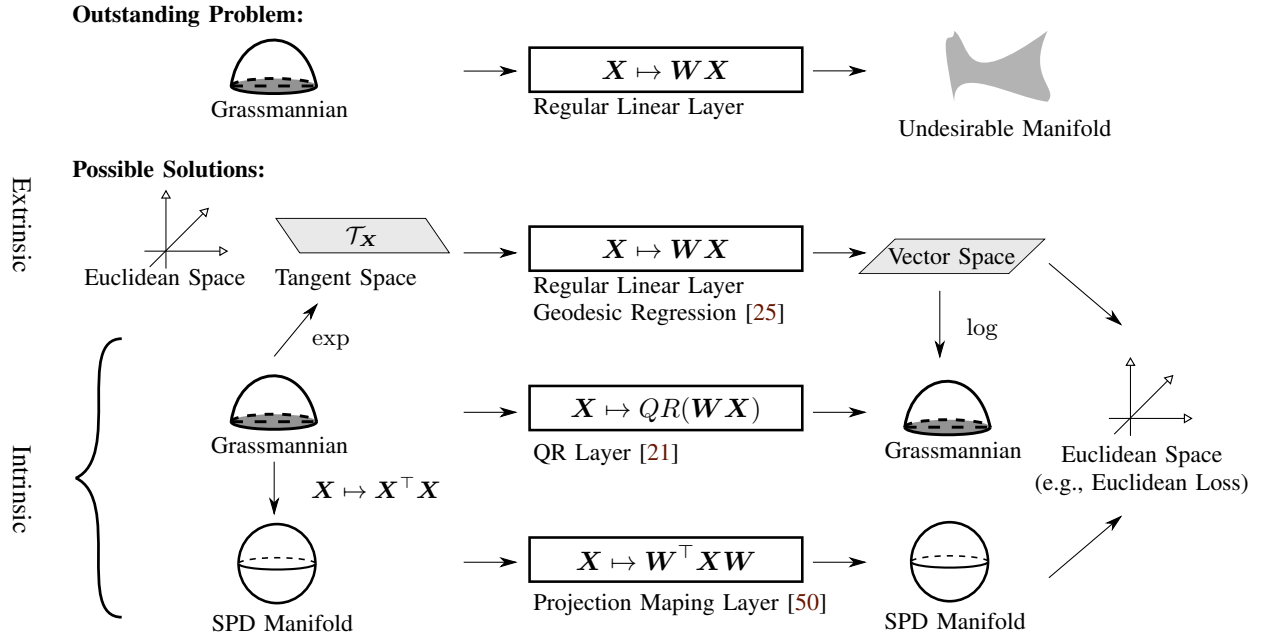


Fig. 10: The problem of existing neural networks and different approaches for constructing mapping network layers on the Grassmann manifold.

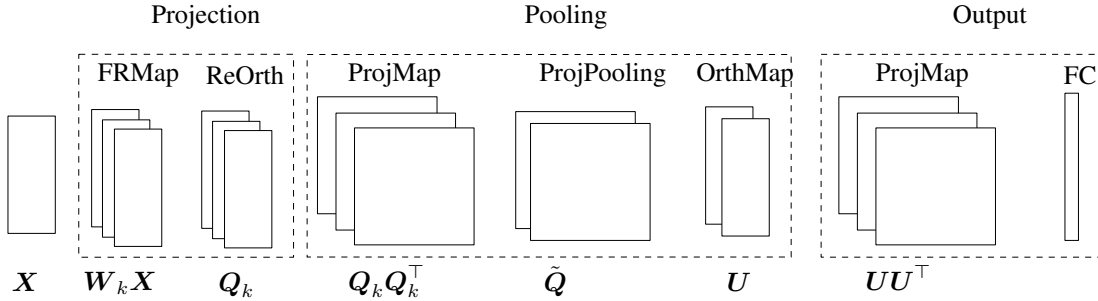


Fig. 11: One design of neural network architecture on Grassmann manifolds (reproduced from [21]). X denotes some Grassmannian data sample fed into the network; W_k is the weights for a particular filter of full rank transform; Q_k is the Q component of the QR decomposition on $W_k X$; \tilde{Q} is the result after average pooling on SPD, i.e., the arithmetic average of $Q_k Q_k^T$ for some filters; U is the eigenspace of \tilde{Q} extracted by eigen decomposition; finally, the output layer is the vectorized output of the final projection layer.

deep neural networks, such tasks usually rely on handcrafted feature extractors such as SIFT, HoG or SURF and a variety of dimensionality reduction techniques. Learning in computer vision, by nature, is closely related to linear subspaces (or Grassmann manifolds). For instance, in a properly chosen subspace, the features of a subject can be invariant under different poses or illuminations and differentiable from those of another subject. Then an image/video recognition problem can be formulated as a discriminant learning problem on the Grassmann manifold (Section III-A). As a concrete example, we consider image-set based emotion classification problem, where we use the dataset, *acted facial expressions in the wild* (AFEW) [51, 52], to demonstrate the algorithm. This dataset contains video clips categorized under sever different emotions (happy, sad, angry, fear, neutral, exciting, surprised). In Fig. 12, the results obtained from GDA introduced in Section III-A are presented. The well-known t -SNE [53] algorithm to applied to visualize the raw data in Fig. 12a and

the discriminant representation learnt from GDA in Fig. 12b. One can observe that GDA recovers the discriminative representations of emotions hidden in high-dimensional raw data.

b) Intelligent Multiple-Input Multiple-Output (MIMO) Communication: MIMO communications has been a key physical technology driving the evolution of wireless systems from 1G to 5G. Its feature is to leverage spatial degrees of freedom generated by antenna arrays to scale up data rates by spatial multiplexing or improve link reliability by spatial diversity [54]. Grassmann manifolds have been exploited in different areas of MIMO communication, most notable applications are non-coherent (Grassmann) MIMO modulation [10] and quantization of precoder feedback [55]. For precoder quantization, precoder codebooks can be generated by quantizing a Grassmann manifold, the space of unitary precoder matrices, using e.g., the Grassmann K-means algorithm. In non-coherent MIMO modulation, a Grassmann constellation consists of a set of points on a Grassmann manifold that are

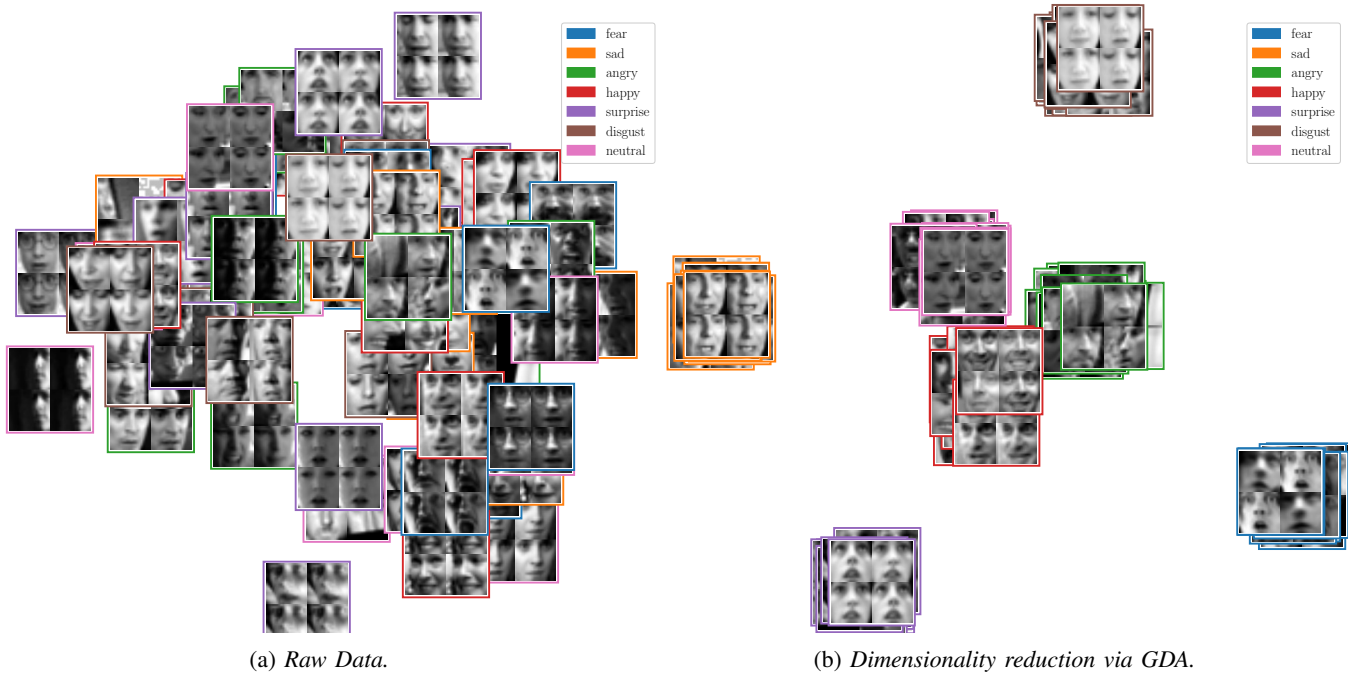


Fig. 12: Emotion classification using Grassmannian learning (GDA) from the AFEW Dataset (best viewed in colour).

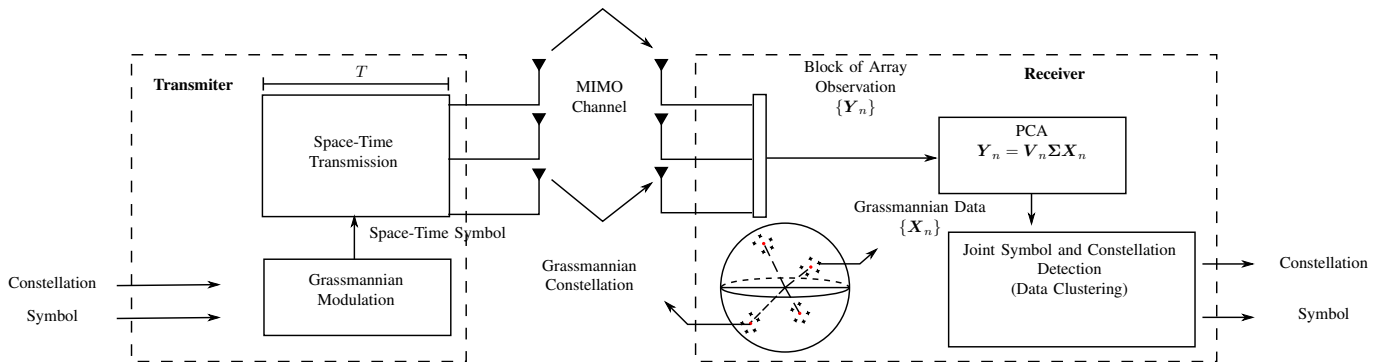


Fig. 13: Automatic recognition of space-time constellation by learning on the Grassmann manifold for an intelligent MIMO communication system.

computed e.g., from subspace packing [11]. In practice, non-coherent MIMO had not been as popular as coherent MIMO as the former cannot scale the data rate by spatial multiplexing as the latter. Nevertheless, recent years have seen the resurgence of non-coherent MIMO in research on next-generation low-latency low-rate machine-type communication as the technique requires no channel training and is robust against fading [56]. Recently, targeting next-generation intelligent MIMO receiver, a framework of automatic recognition of space-time constellation is developed in [12] leveraging algorithms for unsupervised learning on Grassmann manifold originally developed for computer vision. The system proposed in [12] is illustrated in Fig. 13.

c) Recommender Systems: One practical use case of the low-rank representation learning is to build recommender systems using the Grassmannian optimization method for low-rank matrix completion as introduced in Section III-C [57].

The preferences of users on the items can be formed by a *preference matrix*, where the rows and columns represent items and users. The entries are the scores of preferences and the missing entries correspond to unavailable data. For example, in the Netflix Challenge [58], the preferences are the motive ratings by viewers. Then the missing entries can be reconstructed using techniques for matrix completion. An illustration of a recommender system is given in Fig. 14.

VI. CONCLUDING REMARKS

In this paper, we introduced the preliminaries and the shallow and deep paradigms of Grassmannian learning. Relevant techniques have been demonstrated using a set of examples and applications covering areas including computer vision, wireless communications, and recommender systems. Despite the separation into different topics in this paper for the purpose of exposition, shallow and deep Grassmann learning cannot be

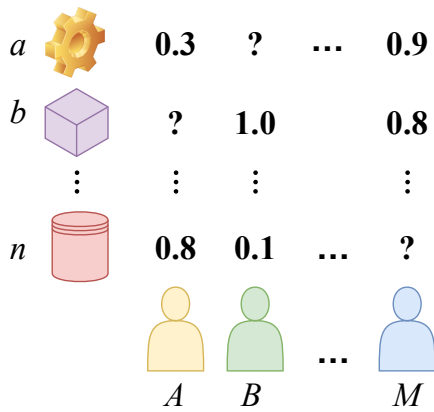


Fig. 14: The matrix-completion problem in recommender systems. Each column of the matrix corresponds to a user, and each row to an item. The entries specify the preference of a user on an item. Under a low-rank constraint on the matrix, the recommender system can predict a missing entry to provide recommendation to a new user.

treated as two separate areas. In contrast, they are interwound where techniques in the former area playing the role of building blocks of the latter. The latest paradigm, Grassmann deep learning, is a nascent but fast growing area with many research opportunities. Some of them are summarized as follows.

- *Embedding Geometry in Deep Neural Networks:* Recent years have seen growing interest in geometry-based deep neural networks, with the potential to become a mainstream approach for improving accuracy and robustness of deep learning. In this direction, Grassmannian learning techniques may play a key role as subspace structural information is embedded in data especially image sets or video. Despite some initial progress [21, 22], geometry based deep neural networks represents a paradigm shift where there are still many open challenges such as overcoming over-fitting by regularization on the Grassmann manifolds, devising more efficient optimizers for non-Euclidean layers, and leverage its power on acquiring intelligence from real-world datasets.
- *General Geometric Deep Learning:* Grassmannian deep learning, a theme of this paper, lies in the general area of geometric deep learning. The area represents a new trend in the deep learning community, which involves deep learning from geometric data including not only images/videos but also other types of data such as 3-dimensional objects, graphic meshes, or social networks [17]. The underpinning basic mathematical toolset is optimization on Riemann manifolds. This area is still largely uncharted.
- *Robust Machine Learning:* One critical weakness of learning models, especially more flexible models such as deep neural networks, is their susceptibility to malicious adversarial perturbations that mislead the models to make incorrect decisions [59, 60]. Grassmannian learning exhibits a certain degree of robustness against small perturbations [33]. The intuitive reason is that it is not

easy for small perturbations to change one subspace to another. Hence it warrants further study on how to leverage Grassmann manifolds (or other Riemann manifolds) to devise more robust machine learning models.

The fast growth of Grassmannian deep learning is assisted by the availability of high-performance software for Riemannian optimization, such as ManOpt [29] for MATLAB and pyManOpt [30] for Python. The software packages render implementation and testing of Grassmannian learning algorithms more accessible to general practitioners in signal processing.

The paper is ended with a hope that this work provides an accessible and inspiring introduction to the area of Grassmann machine learning. Besides an interesting read, readers will be equipped with adequate fundamentals to apply Grassmannian learning to novel scenarios and applications.

REFERENCES

- [1] P. Turaga, A. Veeraraghavan, and R. Chellappa, "Statistical analysis on Stiefel and Grassmann manifolds with applications in computer vision," in Proc. of IEEE Conf. on Computer Vision and Pattern Recognition (CVPR), Anchorage, Jun. 2008.
- [2] P. Turaga, A. Veeraraghavan, A. Srivastava, and R. Chellappa, "Statistical computations on Grassmann and Stiefel manifolds for image and video-based recognition," *IEEE Trans. on Pattern Analysis and Machine Intelligence*, vol. 33, no. 11, pp. 2273–2286, 2011.
- [3] J. Hamm and D. D. Lee, "Grassmann discriminant analysis: a unifying view on subspace-based learning," in Proc. of international conference on Machine learning (ICML), Helsinki, Jul. 2008.
- [4] M. T. Harandi, C. Sanderson, S. Shirazi, and B. C. Lovell, "Graph embedding discriminant analysis on Grassmannian manifolds for improved image set matching," in Proc. of IEEE Conf. on Computer Vision and Pattern Recognition (CVPR), Providence, Jun. 2011.
- [5] L. S. de Souza, H. Hino, and K. Fukui, "3D object recognition with enhanced Grassmann discriminant analysis," in Proc. of Asian Conference on Computer Vision (ACCV), Taipei, Nov. 2016.
- [6] H. E. Cetingul and R. Vidal, "Intrinsic mean shift for clustering on Stiefel and Grassmann manifolds," in Proc. of IEEE Conf. on Computer Vision and Pattern Recognition (CVPR), Miami, Jun. 2009.
- [7] Q. Wang, J. Gao, and H. Li, "Grassmannian manifold optimization assisted sparse spectral clustering," in Proc. of IEEE Conf. on Computer Vision and Pattern Recognition (CVPR), Honolulu, Jul. 2017.
- [8] W. Dai, E. Kerman, and O. Milenkovic, "A geometric approach to low-rank matrix completion," *IEEE Trans. on Information Theory*, vol. 58, no. 1, pp. 237–247, 2012.
- [9] N. Boumal and P.-A. Absil, "Low-rank matrix completion via preconditioned optimization on the Grassmann manifold," *Linear Algebra and its Applications*, vol. 475, pp. 200–239, 2015.
- [10] B. M. Hochwald and T. L. Marzetta, "Unitary space-time modulation for multiple-antenna communications in Rayleigh flat fading," *IEEE Trans. on Information Theory*, vol. 46, no. 2, pp. 543–564, 2000.
- [11] L. Zheng and D. N. C. Tse, "Communication on the Grassmann manifold: A geometric approach to the noncoherent multiple-antenna channel," *IEEE Trans. on Information Theory*, vol. 48, no. 2, pp. 359–383, 2002.
- [12] Y. Du, G. Zhu, J. Zhang, and K. Huang, "Automatic recognition of space-time constellations by learning on the Grassmann manifold," *Submitted to IEEE Trans. on Signal Processing*, 2018. [Online]. Available: arxiv.org/abs/1804.03593
- [13] D. J. Love, R. W. Heath, and T. Strohmer, "Grassmannian beamforming for multiple-input multiple-output wireless systems," *IEEE Trans. on Information Theory*, vol. 49, no. 10, pp. 2735–2747, 2003.
- [14] D. J. Love and R. W. Heath, "Limited feedback unitary precoding for spatial multiplexing systems," *IEEE Trans. on Information Theory*, vol. 51, no. 8, pp. 2967–2976, 2005.
- [15] K. Hall and T. Hofmann, "Learning curved multinomial subfamilies for natural language processing and information retrieval," in Proc. of International Conference on Machine learning (ICML), San Francisco, Jun. 2000.
- [16] Y. LeCun, Y. Bengio, and G. Hinton, "Deep learning," *Nature*, vol. 521, no. 7553, pp. 436–444, 2015.

- [17] M. M. Bronstein, J. Bruna, Y. LeCun, A. Szlam, and P. Vandergheynst, "Geometric deep learning: going beyond Euclidean data," *IEEE Signal Processing Magazine*, vol. 34, no. 4, pp. 18–42, 2017.
- [18] F. Monti, D. Boscaini, J. Masci, E. Rodola, J. Svoboda, and M. M. Bronstein, "Geometric deep learning on graphs and manifolds using mixture model cnns," in Proc. of IEEE Conf. on Computer Vision and Pattern Recognition (CVPR), Honolulu, Jul. 2017.
- [19] J. Masci, D. Boscaini, M. Bronstein, and P. Vandergheynst, "Geodesic convolutional neural networks on Riemannian manifolds," in Proc. of IEEE International Conference on Computer Vision Workshop (ICCVW), Santiago, Dec. 2015.
- [20] B. Poole, S. Lahiri, M. Raghu, J. Sohl-Dickstein, and S. Ganguli, "Exponential expressivity in deep neural networks through transient chaos," in Proc. of Advances in Neural Information Processing Systems (NIPS), Barcelona, Dec. 2016.
- [21] Z. Huang, J. Wu, and L. Van Gool, "Building deep networks on Grassmann manifolds," in Proc. of Association for the Advancement of Artificial Intelligence (AAAI), New Orleans, Feb. 2018.
- [22] S. Herath, M. Harandi, and F. Porikli, "Learning an invariant Hilbert space for domain adaptation," in Proc. of IEEE Conf. on Computer Vision and Pattern Recognition (CVPR), Honolulu, Jul. 2017.
- [23] R. Gopalan, R. Li, and R. Chellappa, "Domain adaptation for object recognition: An unsupervised approach," in Proc. of International Conference on Computer Vision (ICCV), Barcelona, Nov. 2011.
- [24] B. Gong, Y. Shi, F. Sha, and K. Grauman, "Geodesic flow kernel for unsupervised domain adaptation," in Proc. of IEEE Conf. on Computer Vision and Pattern Recognition (CVPR), Providence, Dec. 2012.
- [25] S. Lohit and P. Turaga, "Learning invariant Riemannian geometric representations using deep nets," in Proc. of International Conference on Computer Vision Workshop (ICCVW), Venice, Oct. 2017.
- [26] A. Edelman, T. A. Arias, and S. T. Smith, "The geometry of algorithms with orthogonality constraints," *SIAM Journal on Matrix Analysis and App.*, vol. 20, no. 2, pp. 303–353, 1998.
- [27] P.-A. Absil, R. Mahony, and R. Sepulchre, "Riemannian geometry of Grassmann manifolds with a view on algorithmic computation," *Acta Applicandae Mathematicae*, vol. 80, no. 2, pp. 199–220, 2004.
- [28] —, *Optimization algorithms on matrix manifolds*. Princeton Univ. Press, 2009.
- [29] N. Boumal, B. Mishra, P.-A. Absil, and R. Sepulchre, "Manopt, a Matlab toolbox for optimization on manifolds," *Journal of Machine Learning Research*, vol. 15, pp. 1455–1459, 2014.
- [30] J. Townsend, N. Koep, and S. Weichwald, "Pymanopt: A python toolbox for optimization on manifolds using automatic differentiation," *Journal of Machine Learning Research*, vol. 17, no. 137, pp. 1–5, 2016.
- [31] W. M. Boothby, *An introduction to differentiable manifolds and Riemannian geometry*. Academic Press, 1986, vol. 120.
- [32] Y.-C. Wong, "Differential geometry of Grassmann manifolds," *Proc. of National Academy of Sciences*, vol. 57, no. 3, pp. 589–594, 1967.
- [33] Y. Chikuse, *Statistics on special manifolds*. Springer Science & Business Media, 2012, vol. 174.
- [34] M. T. Harandi, M. Salzmann, S. Jayasumana, R. Hartley, and H. Li, "Expanding the family of Grassmannian kernels: An embedding perspective," in Proc. of European Conference on Computer Vision (ECCV), Zurich, Sep. 2014.
- [35] T. Hastie, R. Tibshirani, and M. Wainwright, *Statistical learning with sparsity: the LASSO and generalizations*. CRC Press, 2015.
- [36] J. P. Cunningham and Z. Ghahramani, "Linear dimensionality reduction: survey, insights, and generalizations," *Journal of Machine Learning Research*, vol. 16, no. 1, pp. 2859–2900, 2015.
- [37] C. M. Bishop, *Pattern recognition and Machine learning*. Springer, 2006.
- [38] G. Baudat and F. Anouar, "Generalized discriminant analysis using a kernel approach," *Neural Computation*, vol. 12, no. 10, pp. 2385–2404, 2000.
- [39] F. R. Chung, *Spectral graph Theory*. American Mathematical Soc., 1997, no. 92.
- [40] A. Y. Ng, M. I. Jordan, and Y. Weiss, "On spectral clustering: Analysis and an algorithm," in Proc. of Advances in Neural Information Processing Systems (NIPS), Vancouver, Dec. 2002.
- [41] U. Von Luxburg, "A tutorial on spectral clustering," *Statistics and Computing*, vol. 17, no. 4, pp. 395–416, 2007.
- [42] J. Shi and J. Malik, "Normalized cuts and image segmentation," *IEEE Trans. on Pattern Analysis and Machine Intelligence*, vol. 22, no. 8, pp. 888–905, 2000.
- [43] C. Lu, S. Yan, and Z. Lin, "Convex sparse spectral clustering: Single-view to multi-view," *IEEE Trans. on Image Processing*, vol. 25, no. 6, pp. 2833–2843, 2016.
- [44] F. R. Bach and M. I. Jordan, "Learning spectral clustering, with application to speech separation," *Journal of Machine Learning Research*, vol. 7, pp. 1963–2001, 2006.
- [45] C. Ionescu, O. Vantzos, and C. Sminchisescu, "Matrix back-propagation for deep networks with structured layers," in Proc. of International Conference on Computer Vision (ICCV), Santiago, Dec. 2015.
- [46] V. M. Patel, R. Gopalan, R. Li, and R. Chellappa, "Visual domain adaptation: A survey of recent advances," *IEEE Signal Processing Magazine*, vol. 32, no. 3, pp. 53–69, 2015.
- [47] K. Simonyan and A. Zisserman, "Very deep convolutional networks for large-scale image recognition," [Online]. Available: arxiv.org/abs/1409.1556, 2014.
- [48] J. Deng, W. Dong, R. Socher, L.-J. Li, K. Li, and L. Fei-Fei, "Imagenet: A large-scale hierarchical image database," in Proc. of IEEE Conf. on Computer Vision and Pattern Recognition (CVPR), Miami, Jun. 2009.
- [49] M. Harandi and B. Fernando, "Generalized backpropagation, etude de cas: Orthogonality," [Online]. Available: arxiv.org/abs/1611.05927, 2016.
- [50] Z. Huang and L. J. Van Gool, "A Riemannian network for SPD matrix learning," in Proc. of Association for the Advancement of Artificial Intelligence (AAAI), San Francisco, Feb. 2017.
- [51] A. Dhall *et al.*, "Collecting large, richly annotated facial-expression databases from movies," 2012.
- [52] A. Dhall, R. Goecke, J. Joshi, K. Sikka, and T. Gedeon, "Emotion recognition in the wild challenge 2014: Baseline, data and protocol," in Proc. of International Conference on Multimodal Interaction (ICMI), Istanbul, Nov. 2014.
- [53] L. v. d. Maaten and G. Hinton, "Visualizing data using t-SNE," *Journal of Machine Learning Research*, vol. 9, no. Nov, pp. 2579–2605, 2008.
- [54] D. Gesbert, S. Hanly, H. Huang, S. S. Shitz, O. Simeone, and W. Yu, "Multi-cell MIMO cooperative networks: A new look at interference," *IEEE Journal on Sel. Areas in Commun.*, vol. 28, no. 9, pp. 1380–1408, 2010.
- [55] D. J. Love, R. W. Heath, V. K. Lau, D. Gesbert, B. D. Rao, and M. Andrews, "An overview of limited feedback in wireless communication systems," *IEEE Journal on Sel. Areas in Commun.*, vol. 26, no. 8, Oct. 2008.
- [56] S. R. Panigrahi, N. Bjorsell, and M. Bengtsson, "Feasibility of large antenna arrays towards low latency ultra reliable communication," in Proc. of IEEE International Conference on Industrial Technology (ICIT), Toronto, Mar. 2017.
- [57] E. J. Candès and B. Recht, "Exact matrix completion via convex optimization," *Foundations of Computational Math.*, vol. 9, no. 6, p. 717, 2009.
- [58] J. Bennett, S. Lanning *et al.*, "The Netflix prize," in Proc. of International Conference on Knowledge Discovery and Data Mining (KDD), San Jose, Aug. 2007.
- [59] C. Szegedy, W. Zaremba, I. Sutskever, J. Bruna, D. Erhan, I. Goodfellow, and R. Fergus, "Intriguing properties of neural networks," [Online]. Available: arxiv.org/abs/1312.6199, 2013.
- [60] I. J. Goodfellow, J. Shlens, and C. Szegedy, "Explaining and harnessing adversarial examples," [Online]. Available: arxiv.org/abs/1412.6572, 2014.